Chapter 4

PALLADIUM-ADDITIVES

4.1 Introduction

Surface additives (potassium, sodium, silicon, phosphorus, sulfur and chlorine) are present on many catalysts and greatly influence product distributions in many reactions, including CO hydrogenation, ammonia synthesis, steam reforming, hydrogenolysis and D_2 exchange [1,2,3]. However, the nature of the promoting or poisoning effect is not well understood. The two major types of interactions the additives exhibit are either structural or electronic (ligand, chemical). For example, alumina prevents sintering of iron in the ammonia synthesis reaction and is considered a structural interaction, and potassium in the CO hydrogenation reaction increases the specific activity of each site. This thesis shows that additives can both chemically and structurally modify the bonding of small molecules (H_2, CO and C_2H_2) to palladium single crystals.

More specifically, the questions this chapter addresses are:

1. How do surface additives interact with palladium single crystals?

2. How do surface additives modify adsorbate bonding?

3. How do surface additives modify palladium's catalytic activity?

These questions are answered by using a wide variety of surface analytical tools to probe the surface. One of these techniques is CO Temperature Programmed Desorption (TPD) which is a chemical probe sensitive to different binding sites and changes in surface electron density. Previous research has shown that different types of surface sites exhibit different chemistry and that differences in heats of adsorption of surface sites are related to their ability for bond breaking or forming required in catalysis. Using this technique in conjunction with LEED, Work Function measurements, TPD of other molecules (H_2 and C_2H_2), Electron Energy Loss Spectroscopy (EELS) and reaction studies, the interaction of the additives with the surface can be understood on an atomic level.

4.2 Results

4.2.1 Pd(111) - Na,Si,P,S,Cl - CO

CO TPD from clean Pd(111) single crystals showed a single peak maximum at 483K for low CO exposures (1×10^{-9} torr, 50 sec). At higher coverages (1×10^{-8} torr, 50 sec) the maximum shifted to 470K with a shoulder at 410K and at saturation coverages (2×10^{-8} torr, 50 sec) the peak had broadened to extend from 270K to 520K with maximum at 330K and 460K (Figure 4.1). Addition of Na, Si, P, S and Cl changed the desorption temperatures markedly. (Unless otherwise noted CO exposures were at 1×10^{-8} torr, 50 seconds.)

Addition of Na increased the desorption temperature of CO from 480K on the clean surface to 590K on the surface with $\Theta_{Na} = .35$ as shown in Figure 4.2. There was no change in the peak shape, but there was a 20% decrease in the peak area.

CO TPD for silane- and silicon-covered surfaces was different than for the sodium covered surface. Silane decomposed on palladium at 550K, at which point hydrogen from the silane desorbed. The silicon AES peak decreased in intensity and no gas-phase silicon fragments were seen in the mass spectrometer, suggesting

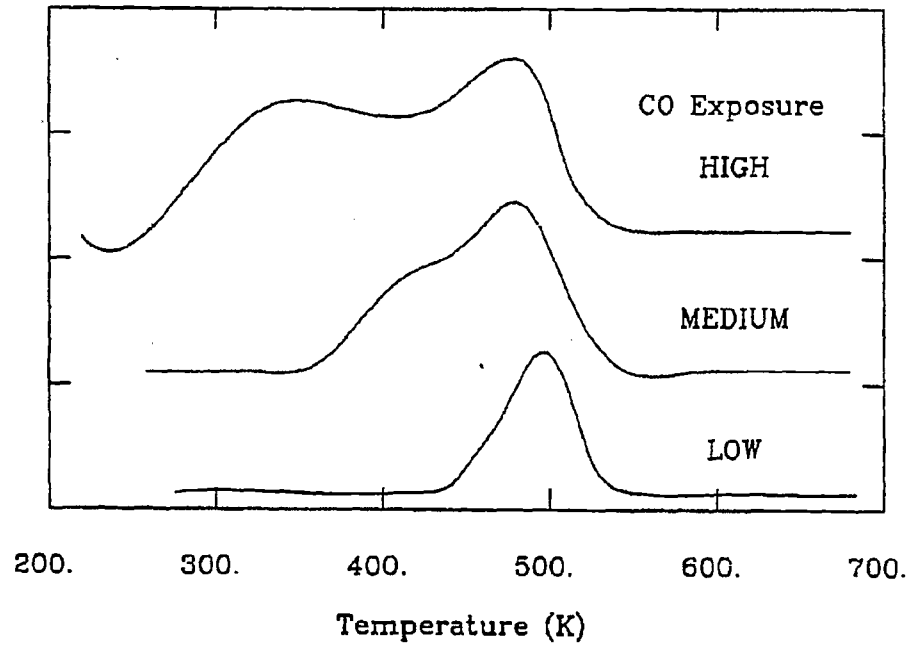

Figure 4.1: CO TPD from clean Pd(111) for low, medium and high CO exposures.

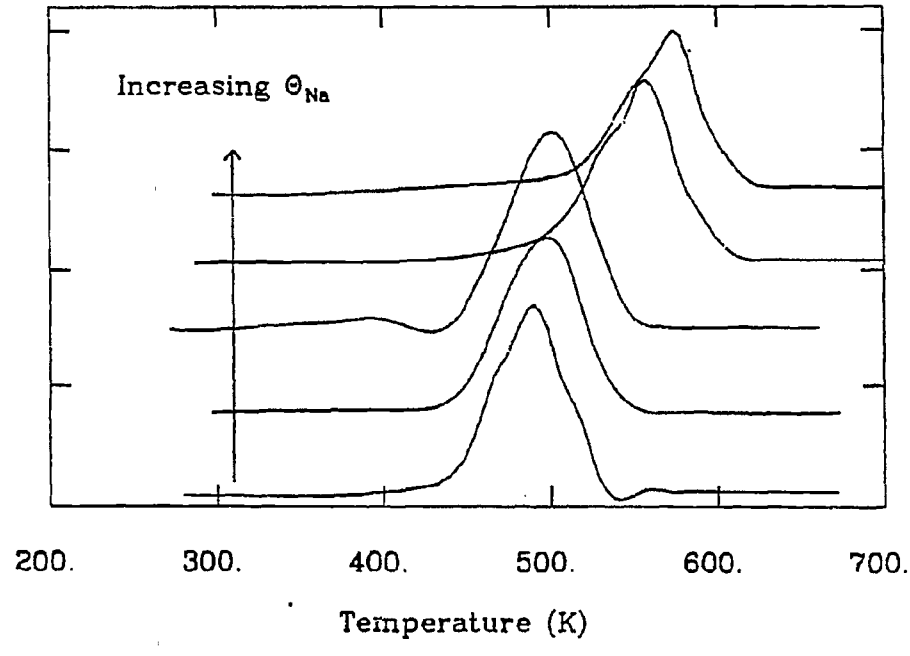

Figure 4.2: CO TPD from sodium-covered Pd(111) for low CO exposures.

that silicon diffused into the bulk. The CO desorption temperature increased as a silane dosed surface was heated repeatedly to 700K. Initially, CO desorbed in a broad peak ranging from 250K to 510K, with maximum at 270K and 390K. Subsequent CO TPD yielded a skewed peak centered at 390K. The third and all other CO TPD that followed for $\Theta_{Si} = .25$ yielded a larger and sharper peak centered at 435K. Sequential silane doses followed by heating shifted the CO desorption peak gradually from 480K ($\Theta_{Si} = 0$) to 420K ($\Theta_{Si} = .36$) (Figure 4.3). With these temperature flashes to 700K, $\Theta_{Si} = .36$ was the maximum obtainable coverage on the palladium surface.

The addition of phosphorus decreased the desorption temperature of CO relative to the Pd(111) surface. As coverages were incremented up to $\Theta_P = .3$ the desorption maximum continuously shifted from 480K ($\Theta_P = 0$) to 465K ($\Theta_P = .3$) (Figure 4.4). At a coverage of $\Theta_P = .35 - .40$ a new peak at 400K appeared, which increased in intensity with increasing phosphorus coverage. At a phosphorus coverage of $\Theta_P = .5$ the high temperature peak disappeared and only the low temperature peak remained, while it also shifted to 370K.

Increasing sulfur coverage decreased the desorption temperature of CO, decreased the peak area, and changed the peak shape as shown in Figure 4.5. At a coverage of $\Theta_S = .34$ the CO desorption shifted from 480K ($\Theta_S = 0$) to 440K with a 23% decrease in the peak area. At higher coverages $.34 < \Theta_S < .47$ a low temperature shoulder grew in and the peak maximum shifted to 380K ($\Theta_S = .43$). The maximum obtainable sulfur coverage ($\Theta_S = .47$) yielded a broad skewed peak,with a desorption maximum at 370K, extending from 300K to 430K.

Addition of chlorine, as in the case of sulfur, decreased the desorption temperature of CO from Pd(111) (Figure 4.6). At low coverages $0 < \Theta_{Cl} < .20$ the maximum was shifted from 480K to 445K, and a low temperature shoulder became evident. At coverages between $\Theta_{Cl} = .22$ and $\Theta_{Cl} = .39$ this shoulder developed

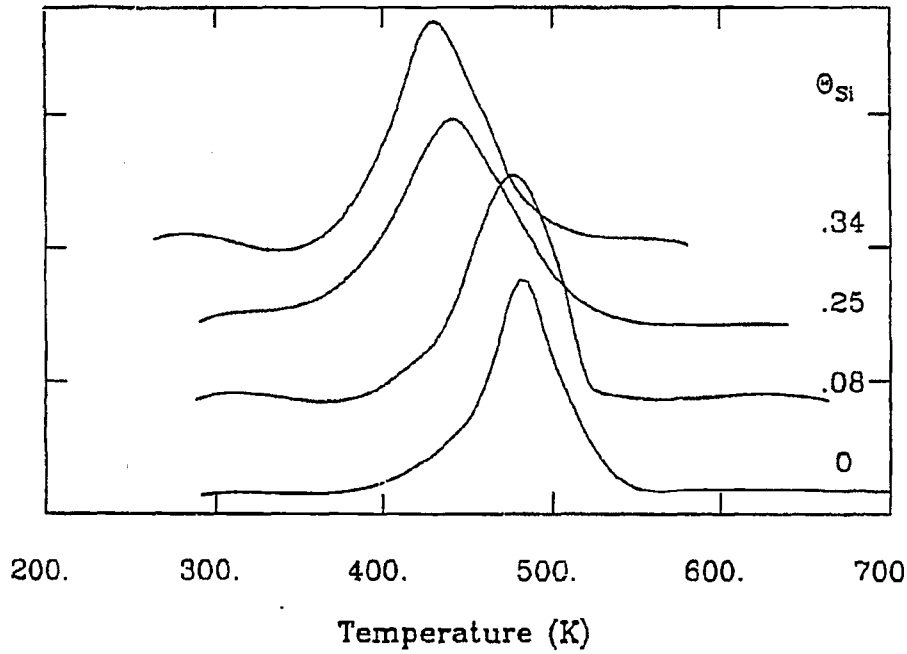

Figure 4.3: CO TPD from a silicon-covered Pd(111) surface for low CO exposures.

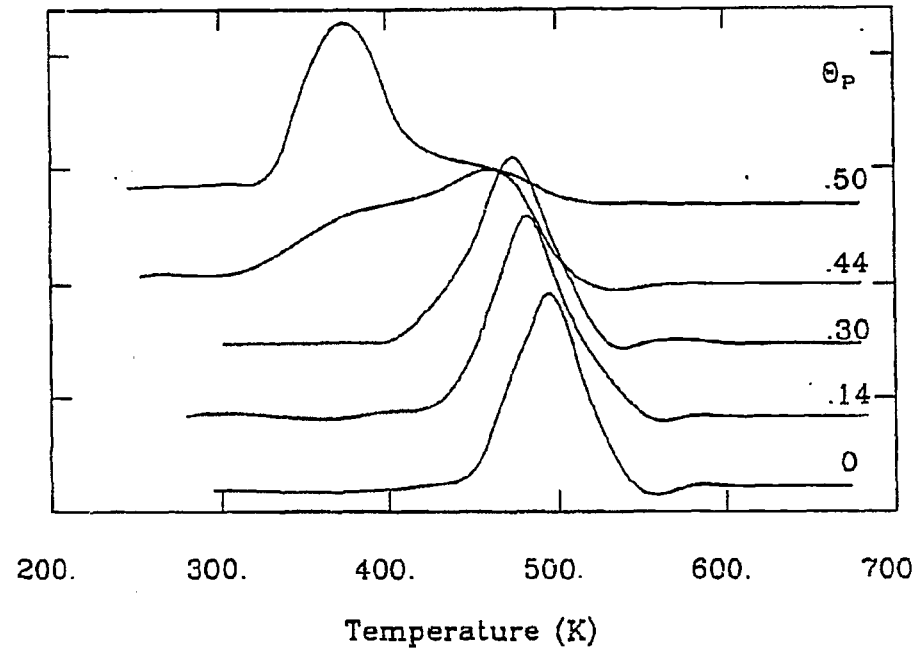

Figure 4.4: CO TPD from a phosphorus-covered Pd(111) surface for low CO exposures.

into a broad peak centered at 340K extending over a range of 150K.

4.2.2 Pd(111) - Si,P,S,Cl - H_2

Hydrogen desorbs from clean Pd(111), with a maximum rate at 310K in a single peak extending over a 100K range. The addition of the surface additives did not appreciably change the peak maximum or shape, but only decreased the amount of hydrogen that adsorbed on the surface. Figure 4.7 shows the relative change in desorbing hydrogen as a function of additive coverage. Chlorine showed the largest decrease in hydrogen chemisorption followed by sulfur, phosphorus and then silicon.

4.2.3 Pd(100) - K,Si,P,S,Cl - CO

CO TPD traces from clean Pd(100) surfaces show a single peak maximum at 470K at low coverages (1×10^{-9} torr, 50 sec) (Figure 4.8). Increasing CO exposures (1×10^{-8} torr, 50 sec) shifted the maximum to 420K with a low temperature shoulder at 390K. At saturation coverages (2×10^{-8} torr, 50 sec) the peak had a maximum at 420K with a well defined shoulder at 360K.

Potassium increased the CO desorption temperature maximum. At low potassium coverages ($\Theta_K = 0 \rightarrow .2$) the CO maximum shifts from 470K to 560 with broadening (Figure 4.9). At higher coverages ($\Theta_K > .35$) a sharp CO peak evolves at 620K. As the potassium concentration is increased this peak becomes larger relative to the 560K peak.

On the silicon covered surface the CO desorption maximum shifted to lower temperatures relative to clean Pd. Trace quantities of silicon ($\Theta_{Si} = .05$) shifted the maximum by 80° to 390K for low CO exposures. Medium CO exposures showed a maximum at 360K (Figure 4.10). Further additions of silicon ($.1 < \Theta_{Si} < .35$) gradually shifted the maximum down to 320K ($\Theta_{Si} = .35$) for low CO

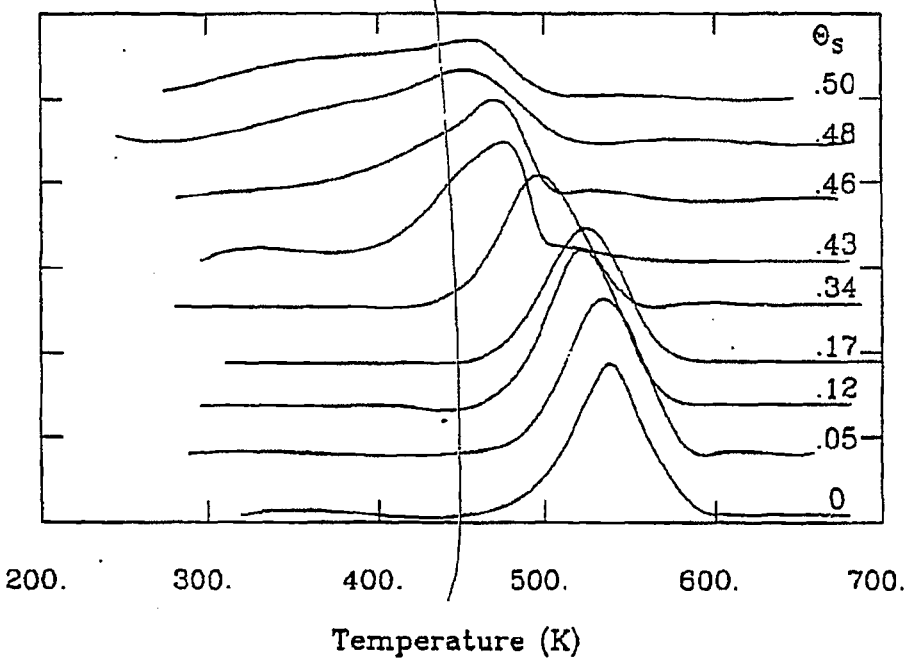

Figure 4.5: CO TPD from a sulfur-covered Pd(111) surface for low CO exposures.

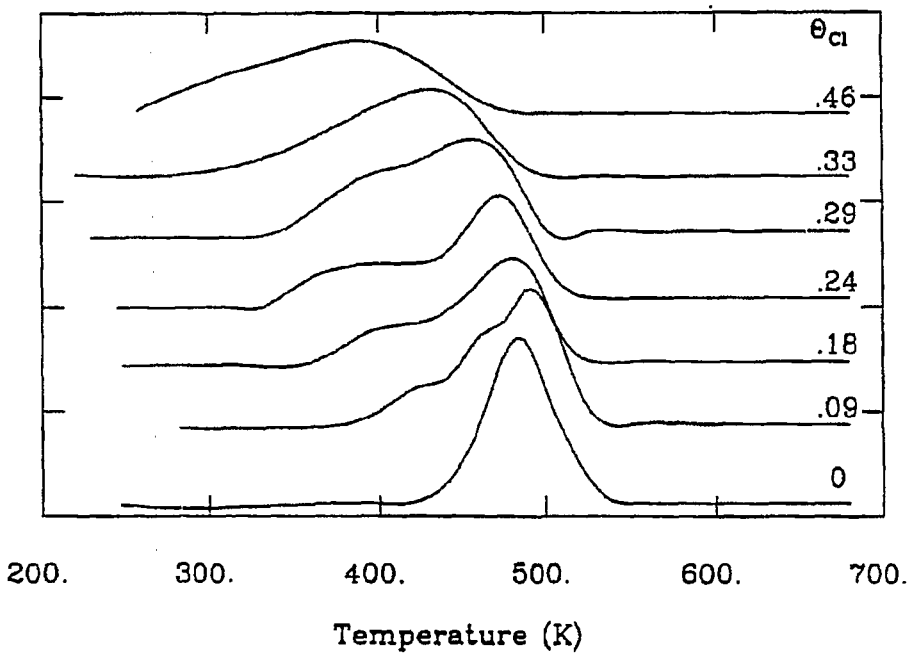

Figure 4.6: CO TPD from a chlorine-covered Pd(111) surface for low CO exposures.

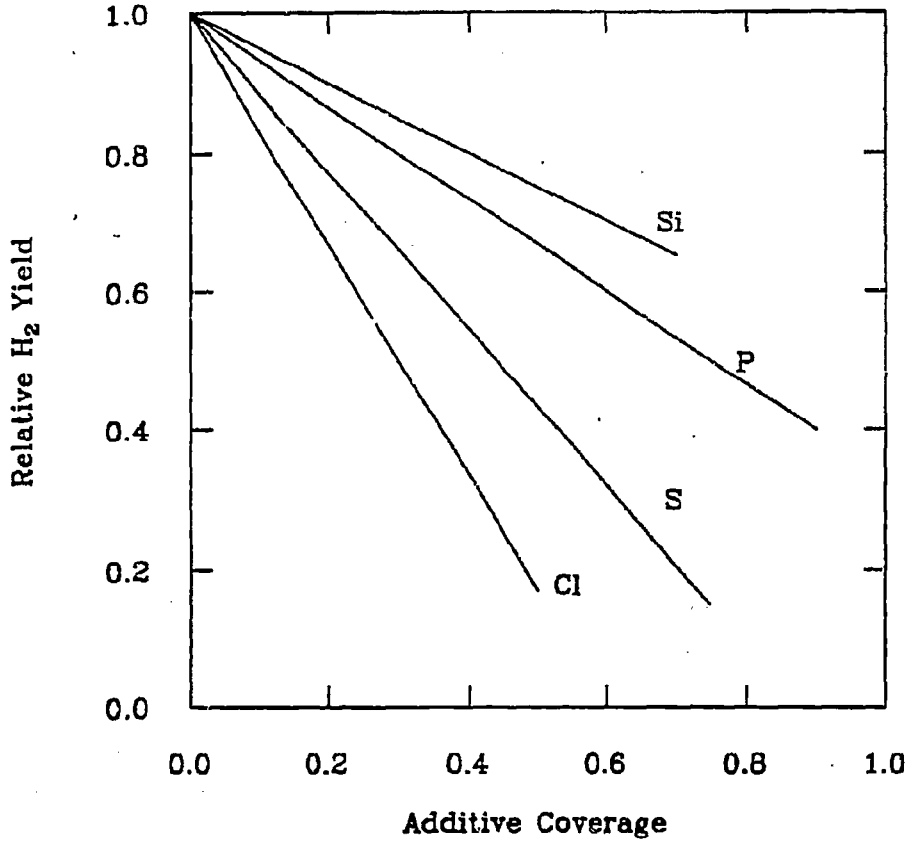

Figure 4.7: Relative amount of hydrogen desorbing from the additive-covered Pd(111) surface.

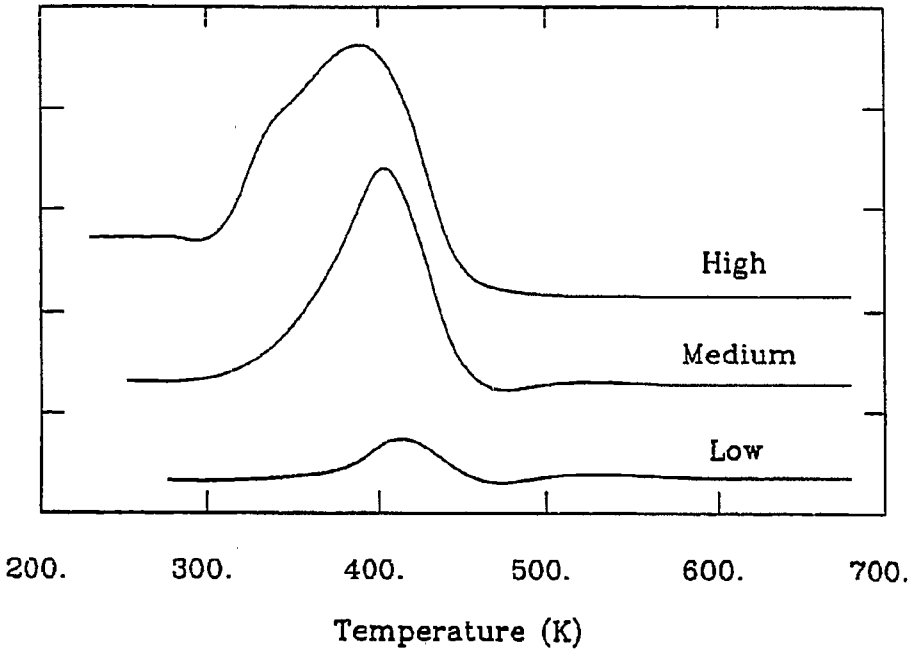

Figure 4.8: CO TPD from a clean Pd(100) surface for low, med and high CO exposures.

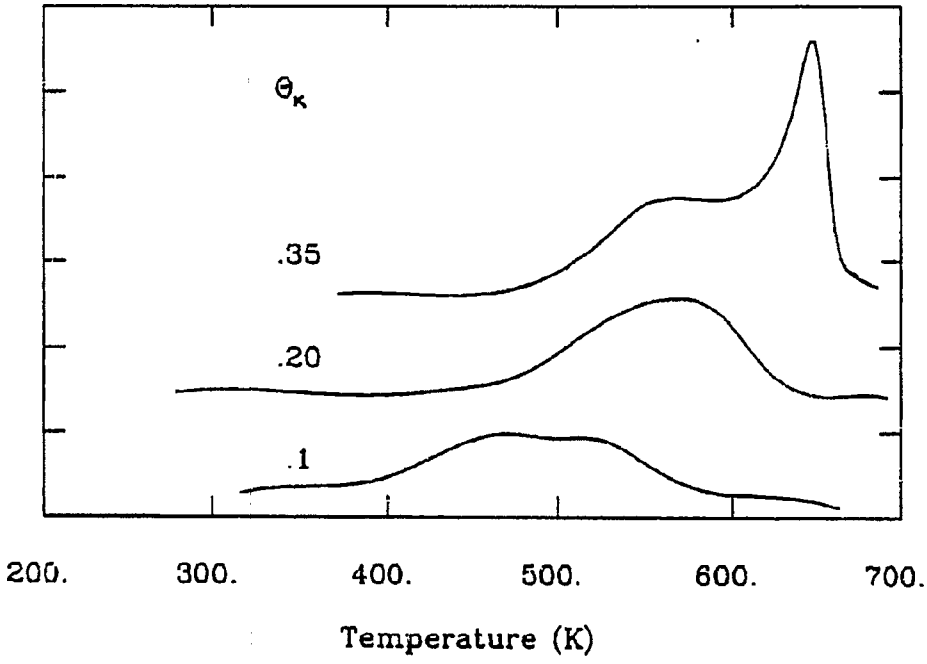

Figure 4.9: CO TPD from a potassium-covered Pd(100) surface for low CO exposures.

exposures (1×10^{-9} torr, 50 sec) and 260K at high (2×10^{-8} torr, 50 sec) exposures. No major changes in either the peak area or shape were observed.

Addition of phosphorus to the Pd(100) surface decreased CO desorption temperatures with peak broadening (Figure 4.11). At low coverages ($\Theta_P = .1$) the CO maximum were at 420K, 400K and 390K (340K shoulder) for low (1×10^{-9} torr, 50 sec), medium (1×10^{-8} torr, 50 sec) and high (2×10^{-8} torr, 50 sec) exposures of CO respectively. At higher coverages ($\Theta_P = .25$), the maximum was shifted to 370K for low CO exposures.

Sulfur lowered the CO desorption maximum, changed the peak shape and also decreased the amount of adsorbed CO (Figure 4.12). At low coverages , $0 < \Theta_S < .1$ the CO maximum were shifted to 420K, 390K and 380K for low, medium and high CO exposures. At sulfur coverages between $.1 < \Theta_S < .25$ a low temperature shoulder developed which evolved into the major peak centered at 330K, 310K and 310K for low (1×10^{-9} torr, 50 sec), medium (1×10^{-8} torr, 50 sec) and high high) CO exposures. For $\Theta_S > .25$ this new peak continued to shift to lower desorption temperatures reaching 240K at the maximum obtainable sulfur coverage of $\Theta_S = .6$.

Increasing chlorine concentration on the Pd(100) surface decreased the desorption temperatures of CO without changing peak shape up to $\Theta_{Cl} = .25$ (Figure 4.13). At $\Theta_{Cl} = .21$ the CO maximum at low CO exposures was shifted from 470K ($\Theta_{Cl} = 0$) to 310K ($\Theta_{Cl} = .21$). For higher CO exposures the maximum was shifted to 300K and 290K (1×10^{-8} torr, 50 sec and 2×10^{-8} torr, 50 sec doses respectively). At high chlorine coverages ($\Theta_{Cl} = .32$) all CO exposures yield the same double peak (195K and 285K) CO desorption trace.

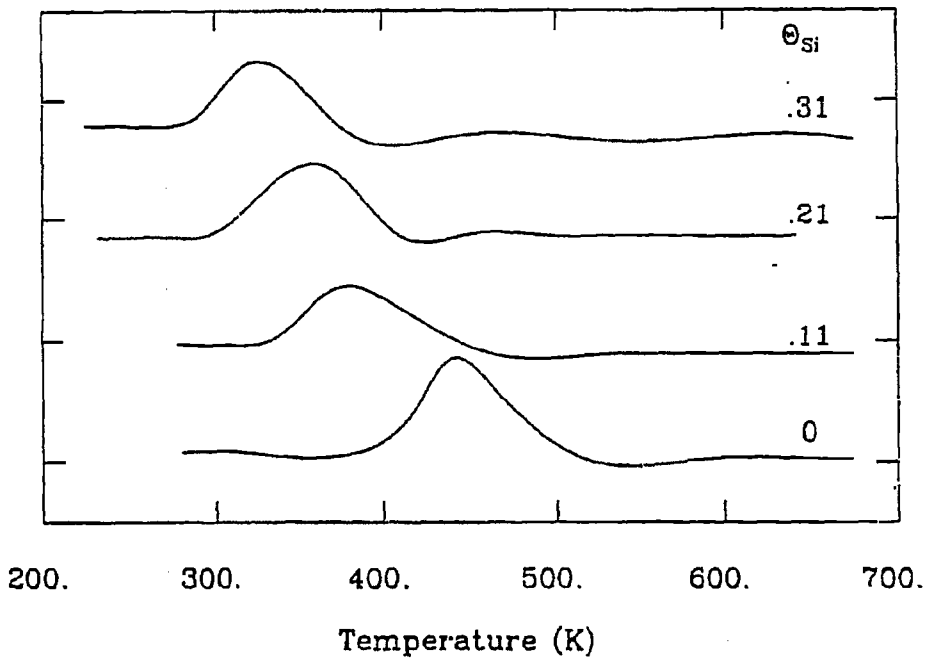

Figure 4.10: CO TPD from a silicon-covered Pd(100) surface for lo CO exposures.

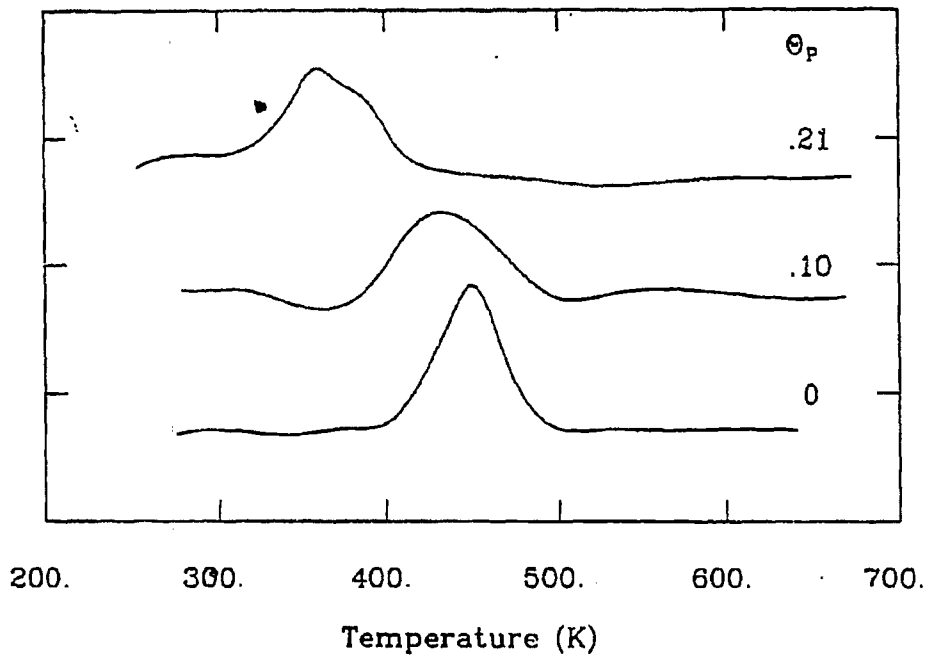

Figure 4.11: CO TPD from a phosphorus-covered Pd(100) surface for low CO exposures.

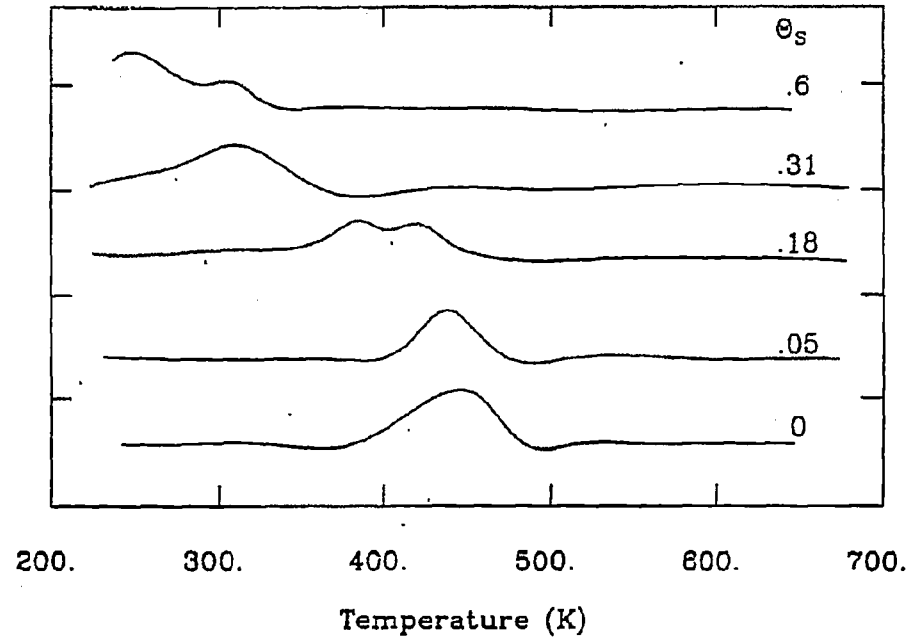

Figure 4.12: CO TPD from a sulfur-covered Pd(100) surface for low CO exposures.

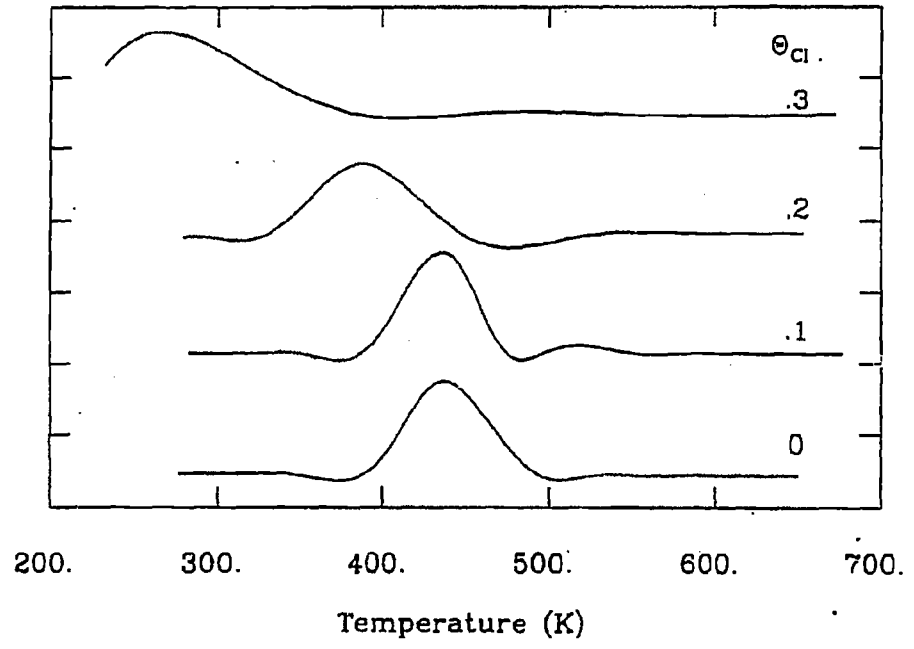

Figure 4.13: CO TPD from a chlorine-covered Pd(100) surface for low CO exposures.

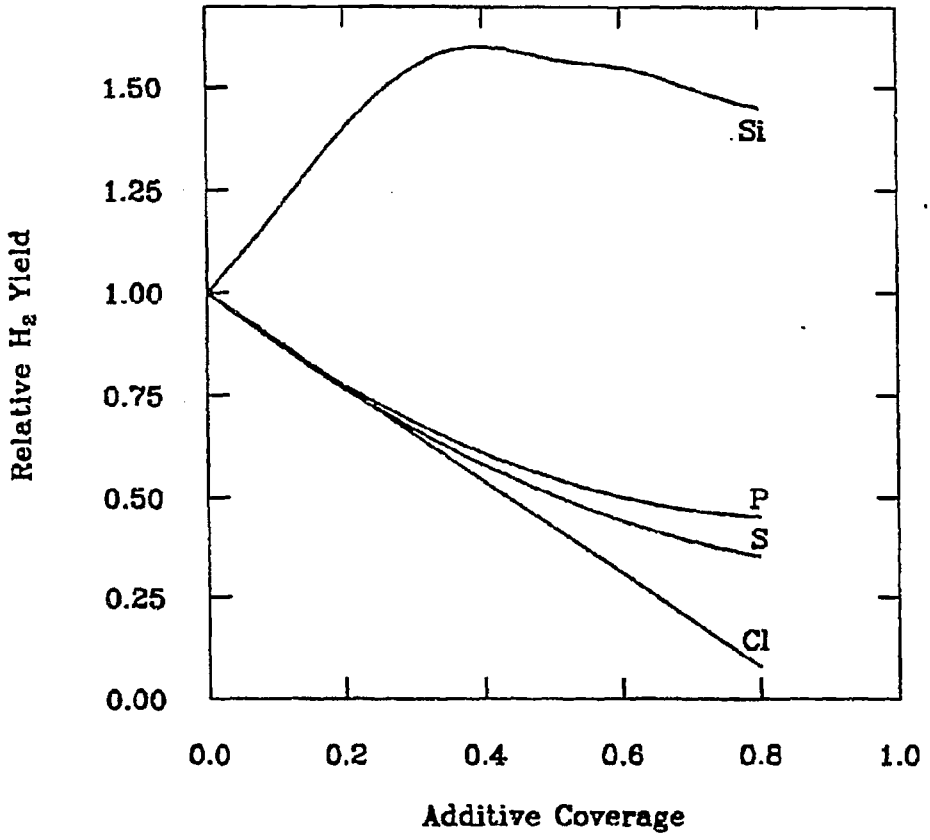

Figure 4.14: Relative amount of hydrogen desorbing from the additive-covered Pd(100) surface. Silicon increases the sticking coefficient of hydrogen whereas the other additives decrease the sticking coefficient on this palladium surface.

4.2.4 Pd(100) - Si,P,S,Cl - H_2

Figure 4.14 shows the relative amount of hydrogen desorbing from the additive covered Pd(100) surface. The desorption maximum at 310K of hydrogen from clean Pd(100) is independent of additive coverage. The addition of phosphorus, sulfur and chlorine decreased the amount of chemisorbed hydrogen (decreasing peak area), whereas silicon increased ($\Theta_{Si} = .4$) the amount of hydrogen by 60%.

4.2.5 Pd(110) - Na,Si,P,S,Cl - CO

The Pd(110) surface dosed with CO showed a single CO desorption maximum at 440K and 430K for low (1×10^{-9} torr, 50 sec) and medium (1×10^{-8} torr, 50 sec) coverages. At high CO exposures there was a maximum at 430K with a shoulder at 350K and also a new peak at 270K (Figure 4.15). Surface additives were found to modify CO bonding to the surface as outlined below.

Addition of sodium on the (110) surface decreased the desorption temperature of CO, in contrast to the Pd(111) and Pd(100) surfaces (Figure 4.16). At low coverages ($\Theta_{Na} < .2$) the maximum was shifted from 430K to about 400K with a slight (10%) decrease in peak area. At higher coverages ($\Theta_{Na} > .2$) a new low temperature desorption peak at 350K appears (original peak shifted to 385K)[1]. Similar results were observed for potassium on this surface.

Silicon on Pd(110) shifted the CO desorption maximum to lower temperatures (Figure 4.17) without changing the peak shape. At low CO exposures (1×10^{-9} torr, 50 sec) CO desorbs at 350K and for medium exposures the maximum is at 320K for a silicon coverage of $\Theta_{Si} = .44$. For these high silicon coverages, high CO exposures yielded a broad (200°) peak centered at 310K and skewed toward higher temperatures. At intermediate silicon coverages ($\Theta_{Si} = .20 - .30$) the CO maximum is at 370K with a shoulder at 285K, one-fifth as intense.

Phosphorus on the Pd(110) surface had little effect on CO chemisorption at any phosphorus coverage (Figure 4.18). At low CO exposures the CO maximum shifted from 430K to 410K. For medium exposures there were negligible changes in peak area and the desorption maximum shifted from 410K ($\Theta_P = 0$) to 400K ($\Theta_P = .53$). At high CO exposures the low temperature CO peak at 270K was shifted to higher temperature, yielding a broad 210° peak with maximum at 310K and 420K. Doubling this CO exposure (2×10^{-8} torr, 100 sec.) populated the low

[1] Electron beam-induced sodium desorption makes coverage determination difficult.

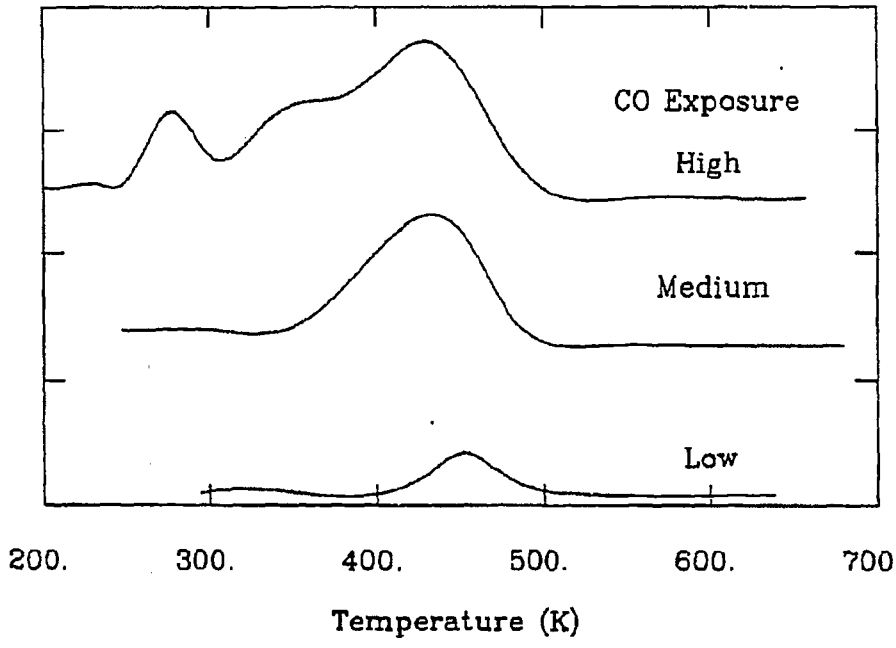

Figure 4.15: CO TPD from a clean Pd(110) surface for low CO exposures.

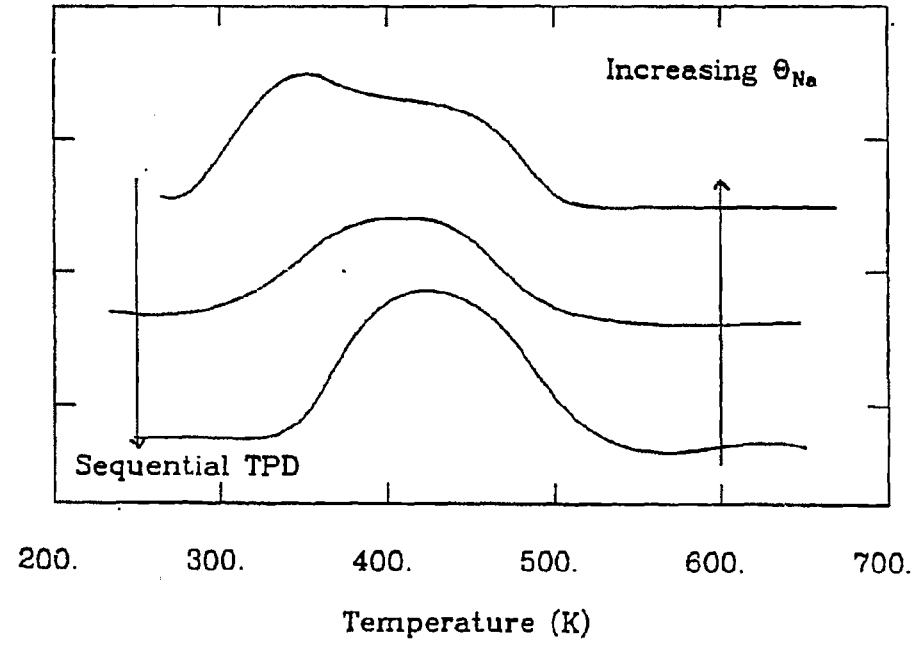

Figure 4.16: CO TPD from a sodium-covered Pd(110) surface for low CO exposures.

temperature side of the broad peak with a new peak at 260K.

Low sulfur coverages ($\Theta_S = 0 \rightarrow .39$) on the Pd(110) surface shift the CO desorption maximum 50K lower in temperature relative to the clean surface (Figure 4.19). At higher sulfur coverages a new low temperature CO desorption peak at 340K appears which increases in intensity relative to the high temperature (420K peak). Increasing sulfur coverages shift the peak to 270K ($\Theta_S = .5$).

The presence of chlorine adsorbed on Pd(110) changed the shape and temperature of CO TPD traces (Figure 4.20). For low CO exposures (1×10^{-9} torr, 50 sec) the peak maximum shifted from 430K to 320K with a peak twice as wide ($\Theta_{Cl} = 0 \rightarrow .32$). At coverages above $\Theta_{Cl} = .32$ this broad peak separated into two equivalent peaks centered at 270K and 330K. For medium CO exposures the maximum at 430K is shifted to 330K and becomes a shoulder on a peak approximately 1.5 times larger centered at 260K. Increasing CO exposures populated the low temperature 260K desorption peak.

4.2.6 Pd(110) - Si,P,S,Cl - H_2

The TPD of hydrogen on additive covered Pd(110) showed no temperature shifts, only peak area changes. Figure 4.21 shows the relative amount of hydrogen desorbing as a function of additive coverage. Silicon has the largest hydrogen chemisorption blocking effect, followed by chlorine, sulfur and phosphorus. It is interesting to note that silicon did not lie above phosphorus as would be expected from relative positions in the periodic table of the elements.

4.2.7 Pd(100) - K,Si,P,S,Cl - Work Function

To observe how the surface electronegativity changes with the addition of different adatoms to the surface, work function measurements were performed on Pd(100) (Figure 4.22). The decrease in work function is greatest for potassium, indicating

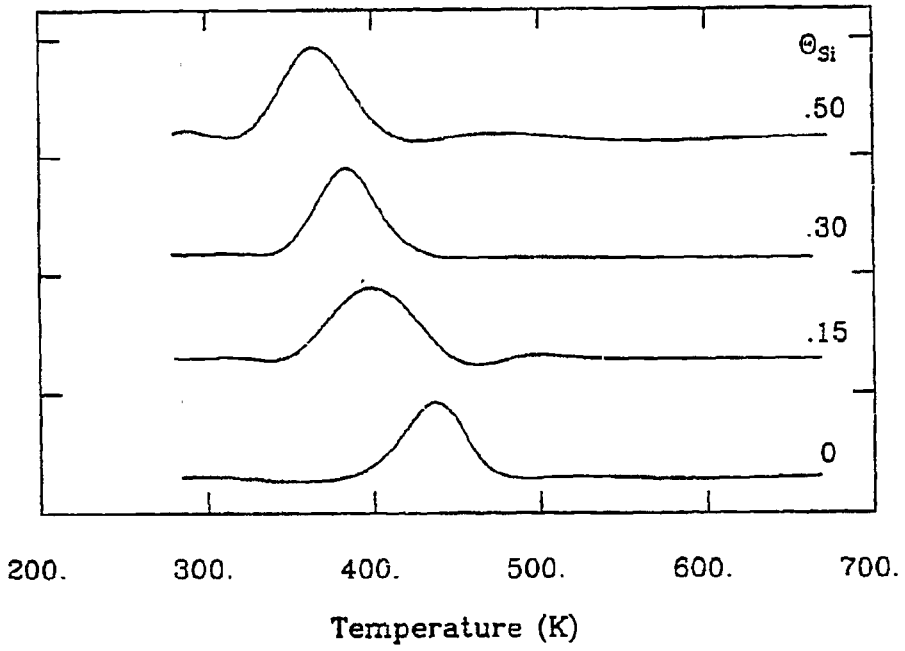

Figure 4.17: CO TPD from a silicon-doped Pd(110) surface for low CO exposures.

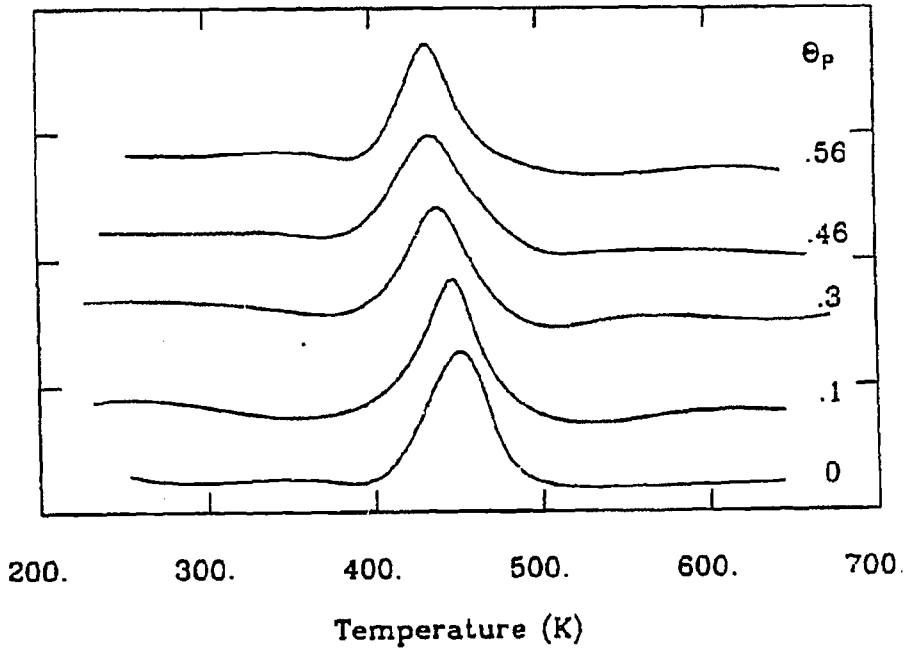

Figure 4.18: CO TPD from a phosphorus-covered Pd(110) surface for low CO exposures.

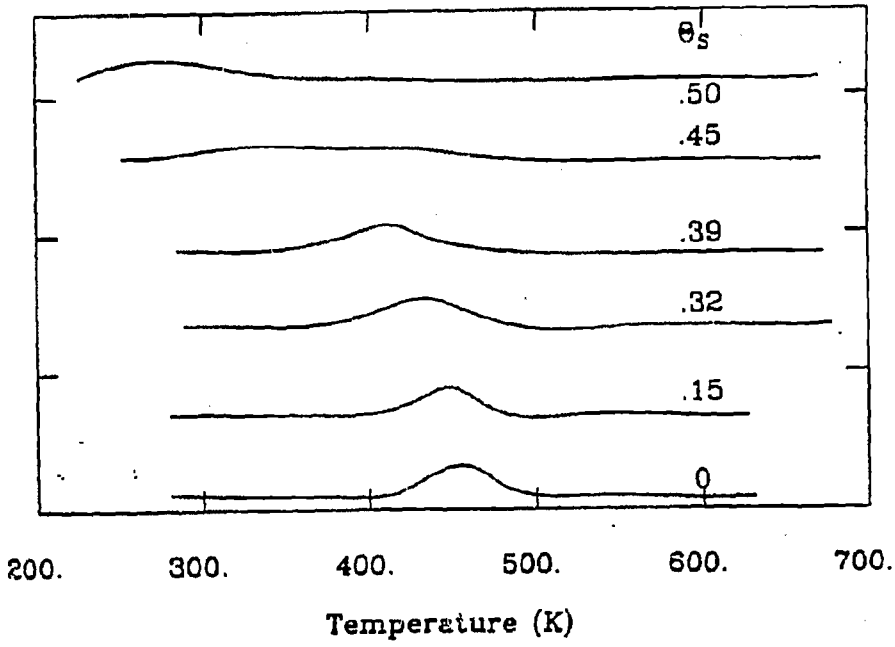

Figure 4.19: CO TPD from a sulfur-covered Pd(110) surface for low CO exposures.

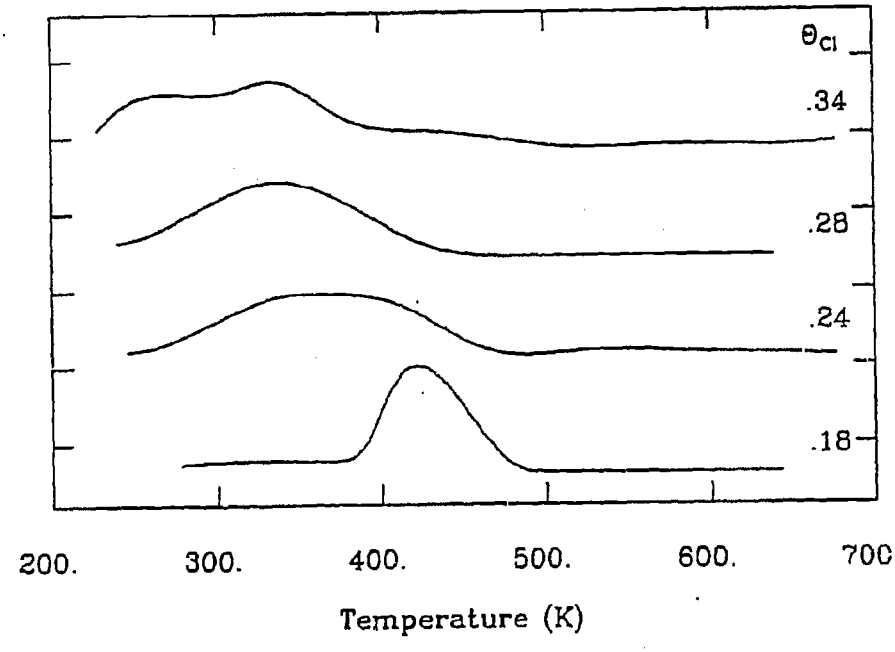

Figure 4.20: CO TPD from a chlorine-covered Pd(110) surface for low CO exposures.

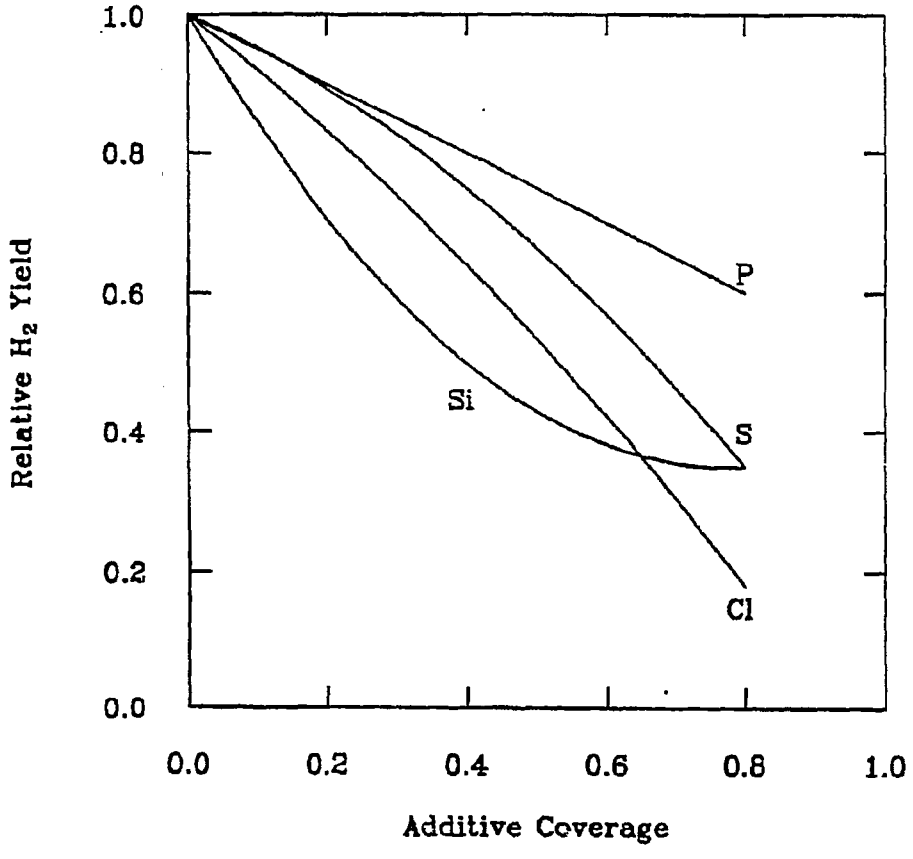

Figure 4.21: The relative hydrogen sticking coefficients on additive covered Pd(110) is shown here. Silicon has the largest hydrogen chemisorption blocking effect followed by chlorine, sulfur and phosphorus.

that it donates the most electron density to the surface per unit coverage, followed by silicon and then phosphorus. Conversely, sulfur increased the work function, implying that it withdraws electron density from the surface.

For silicon, heating the sample to 770K increased the work function by .75 eV (closer to clean Pd(100)), while only slightly decreasing the Pd-Si AES ratio (Figure 4.23). Since no silicon-containing fragments were distinguishable in the mass spectrum, the silicon diffused into the near-surface region of the crystal. This change in work function after sample flashing or annealing was not found for any other surface additive on Pd(100).

4.2.8 LEED

A study of surface ordering was undertaken in this research. Some of the additives were found to order on the palladium single crystal surfaces studied. A complete literature survey of K, Na, Si, P, S and Cl ordering on the Pd(111), (100) and (110) surfaces is presented in Table 4.1.

Phosphorus orders on both the (111) and (110) surfaces. On the (111) surface a $(\sqrt{7} \times \sqrt{7})R17°$ structure forms at low coverages. The spots sharpen at higher coverages ($\Theta_P > .3$) (Figure 4.24). Ordered LEED patterns were also observed for the silicon-covered (100) and (110) surfaces (Figure 4.25). The streaking of the diffraction spots in one direction for silicon on the (110) surface indicate preferential ordering in one direction.

4.2.9 Pd(111) - S - CO (EELS)

Electron Energy Loss Spectroscopy (EELS) was used to study CO adsorbed on clean and sulfur modified Pd(111) surface. The EELS spectrum (Figure 4.26) of CO on the clean Pd(111) surface shows two peaks at 1835 and 325 cm^{-1} which can be assigned to the ν_{CO} and ν_{PdC} stretching modes. These frequencies indicate

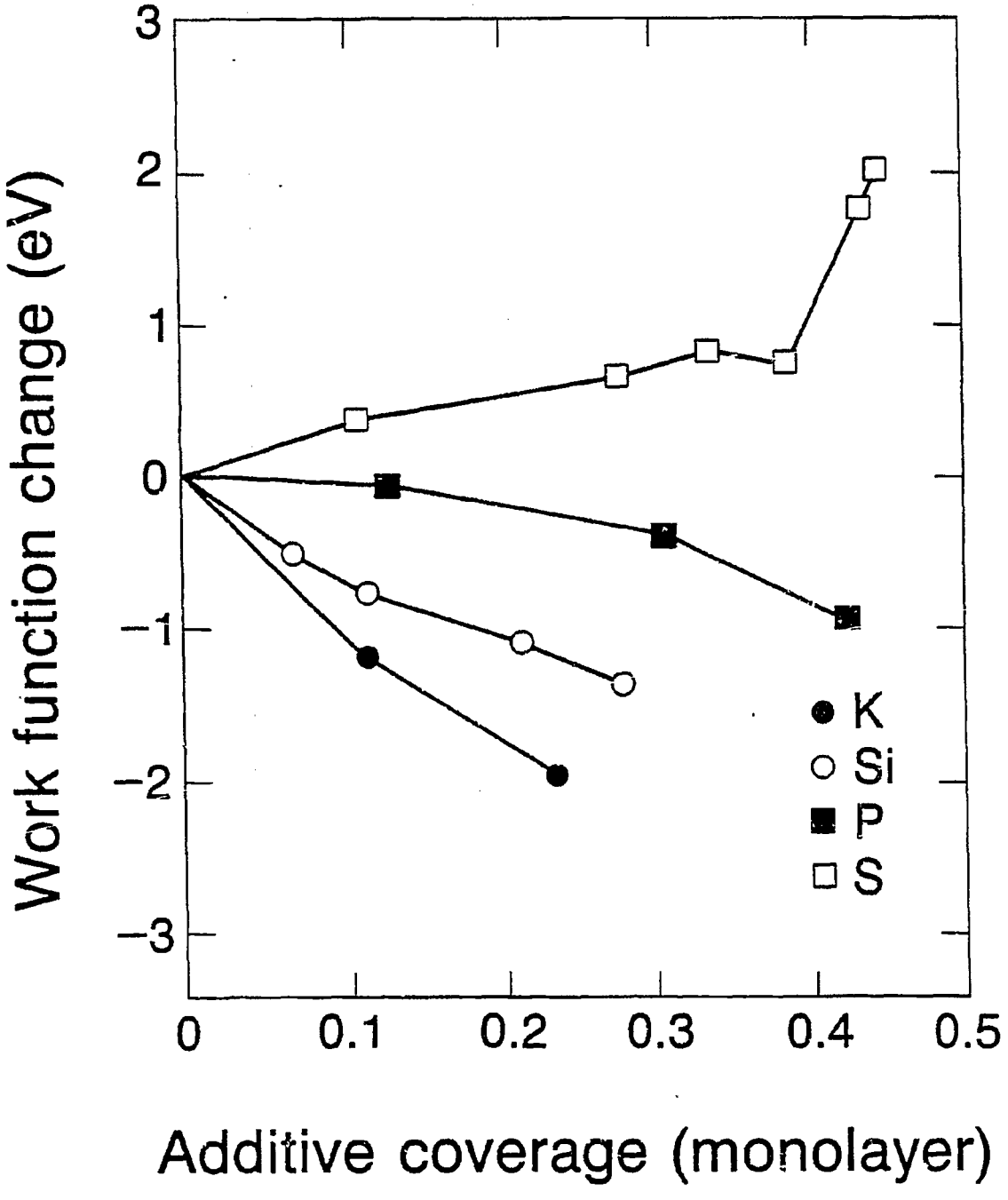

Figure 4.22: Work function changes on the Pd(100) surface in the presence of surface additives is shown here. In general they follow the trend that elements more electronegative than palladium withdraw electron density and increase the work function, and those more electropositive donate electron density and decrease the work function.

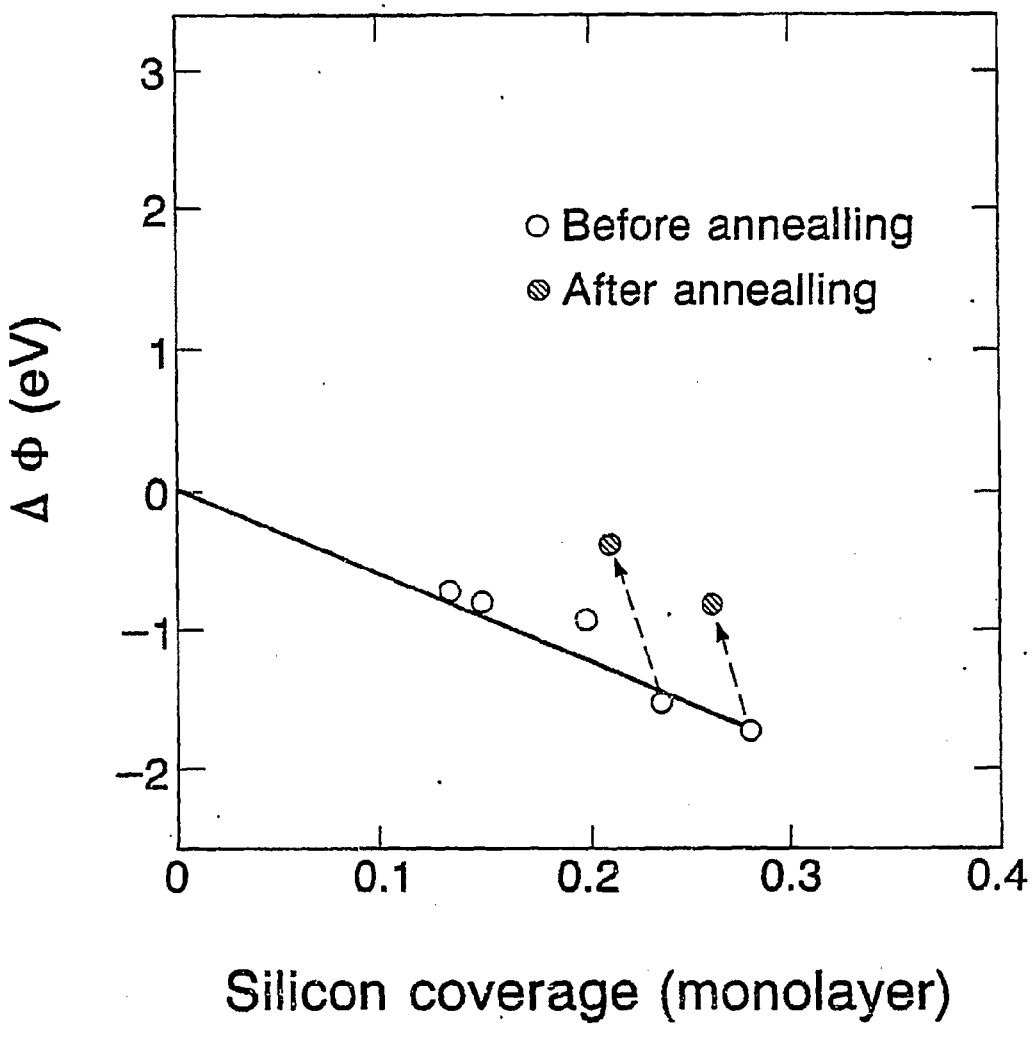

Figure 4.23: On the silicon-covered Pd(100) surface, heating the sample to 770K decreased the work function by .75 eV (closer to the clean surface), while only slightly decreasing the Pd-Si AES ratio.

Additive	Surface		
	(111)	(100)	(110)
CO	$(\sqrt{3} \times \sqrt{3})R30°$ [4]	$(4 \times 2)R45°$ [5]	$c(2 \times 2)$ [4] (4×2)
K, Na			(1×2) reconst.[6]
Si		**Ordered**	**Ordered**
P	$(\sqrt{7} \times \sqrt{7})$**R17°**		**Ordered**
S	$(\sqrt{3} \times \sqrt{3})R30°$	(2×2) [7]	(2×3) [8] $c(2 \times 2)$ $c(8 \times 2)$ (3×2)
Cl	$(\sqrt{3} \times \sqrt{3})R30°$ [9] (3×3)		$c(16 \times 2)$ [10]

Table 4.1: LEED patterns for additives on palladium single crystals.

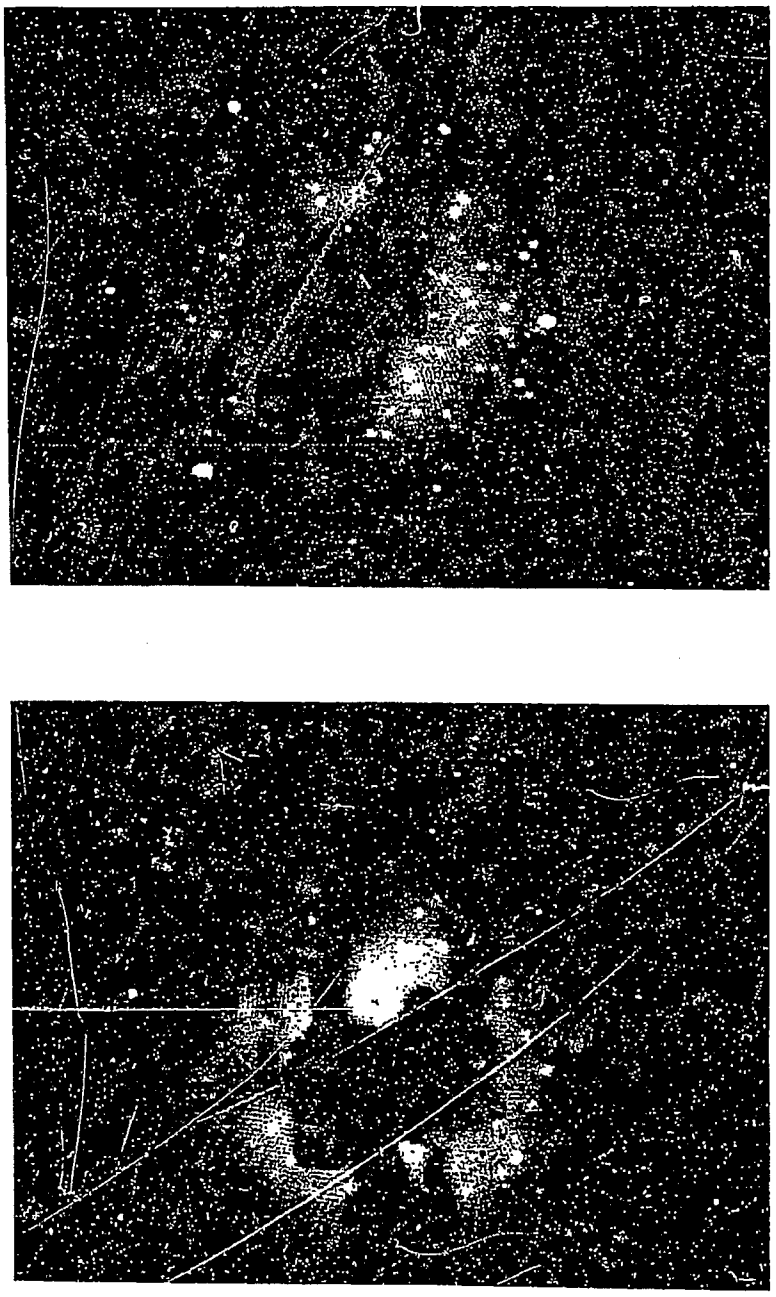

Figure 4.24: The LEED patterns of phosphorus on the (111) ($(\sqrt{7} \times \sqrt{7})R17°$) and (110) surface.

XBB 874-3311

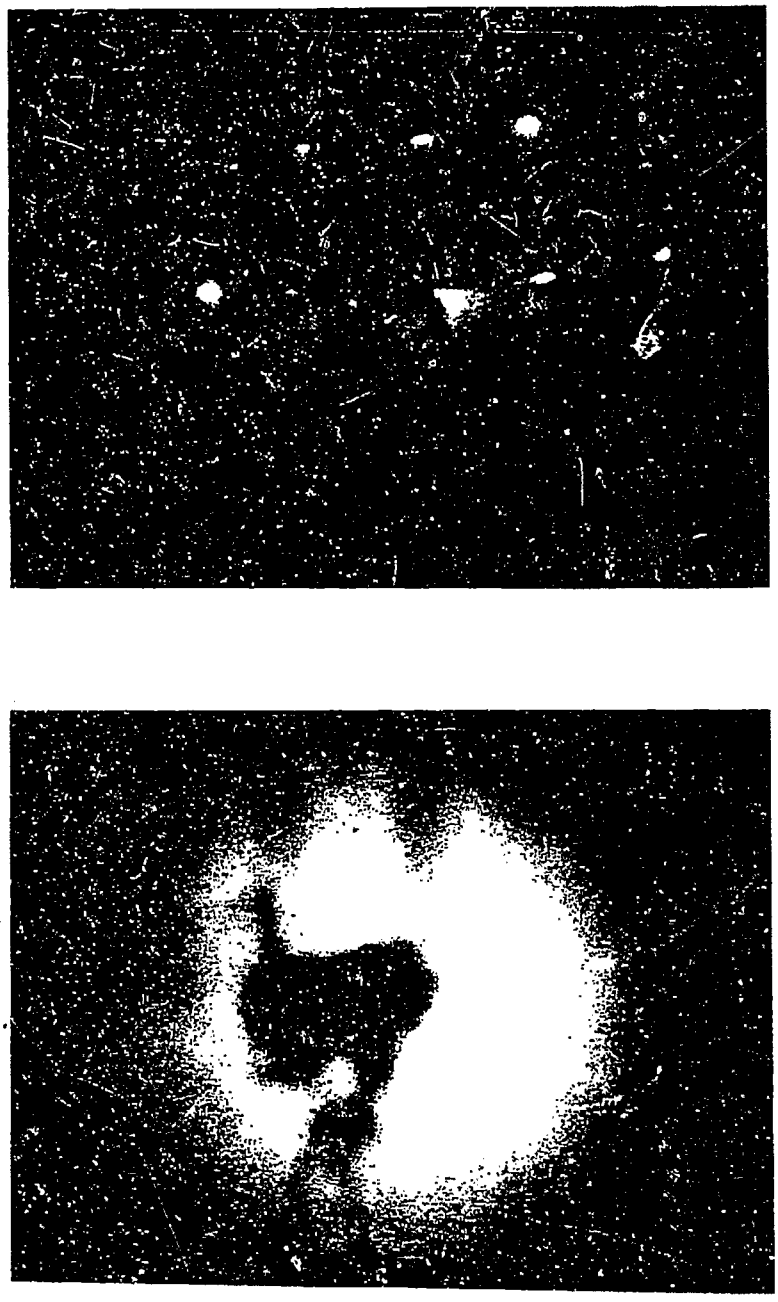

XBB 874-3314

Figure 4.25: LEED patterns of the clean and silicon-covered Pd(110) surface.

a bridged-site position for the molecule. When sulfur ($\Theta_S = .17$) is present on the surface, a new loss peak appears around 740 cm^{-1}, whereas the ν_{CO} frequency shifts down to 1755 cm^{-1}. At higher sulfur coverages this effect is more pronounced and a new low frequency peak can also be seen at 275 cm^{-1}. This latter peak can be assigned to a metal-sulfur stretching mode, similar to what is seen in sulfur-metal complexes [11].

The 740 cm^{-1} peak can be explained by a tilted CO molecule which would allow the δ_{MCO} motion to be EELS active. Some parent metal-carbonyl complexes show such vibrations around 700 cm^{-1} in the infrared spectra: 637 and 644 cm^{-1} for $Ni_2(\pi\text{-}C_5H_5)_2(\mu_2\text{-}CO)_2$ [12], 700 cm^{-1} for $Ru_6C(\mu_2\text{-}CO)(CO)_{16}$ [12] and 600 and 670 cm^{-1} for $Fe_2(\mu_2\text{-}CO)_3(CO)_6$ [13]. The formation of a SCO molecule can be ruled out by comparison to the frequencies of 859, 520 and 2062 cm^{-1} for the ν_{CS}, δ_{OCS} and ν_{CO} respectively [11].

4.2.10 Pd - K,Si,P,S,Cl - C_2H_2

The conversion of acetylene to benzene over palladium single crystals ((111), (100) and (110)) modified with submonolayer quantities of silicon, phosphorus, sulfur, chlorine and potassium has been studied under both ultra-high vacuum and atmospheric pressure conditions [14]. The reaction is structure-sensitive in both pressure regimes, and also proceeds on palladium films and palladium supported on alumina. In UHV the (111) face is the most active, followed by the (110) and (100) surfaces which are 1/8 and 1/20 as active respectively (Figure 4.27) [15]. At high pressures, the (111) and (100) surfaces have equal catalytic activity whereas the (110) face is one-fourth as active. If the percentage of open or active sites is taken into account the reaction exhibits the same structure sensitivity ordering as in UHV.[2]

[2]Percentage of open sites was determined by CO titrations. CO binds only to bare palladium and not to carbon overlayers

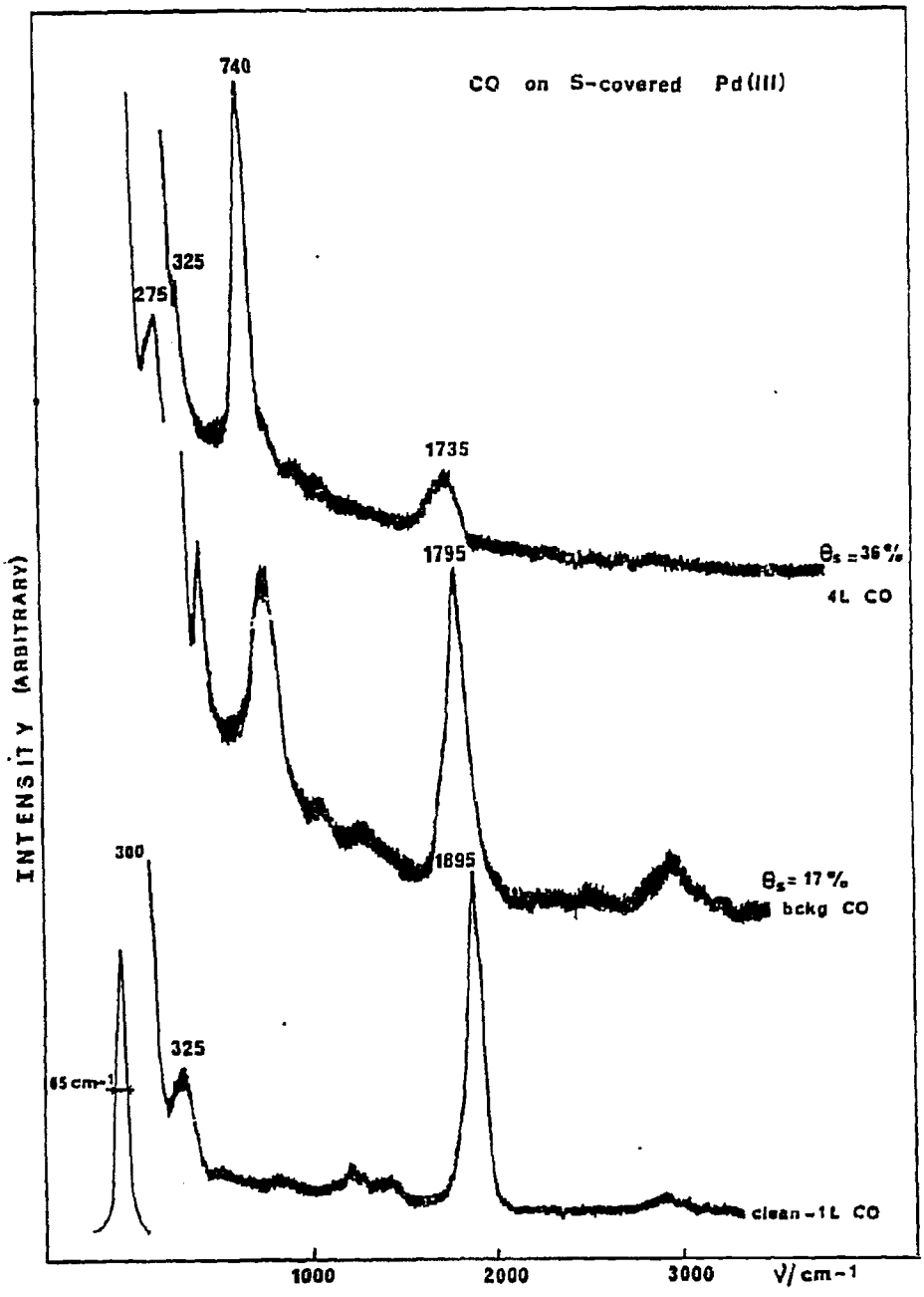

Figure 4.26: The EELS spectra of CO on sulfur-modified Pd(111) is shown here. At higher sulfur coverages new peaks grow in which can be assigned to new CO binding configurations.

At atmospheric pressures electron-donating additives enhanced the rate of benzene formation and electron-accepting additives reduced the rate [14]. It should be noted that on the (111) and (100) surfaces potassium increased benzene formation, whereas on the (110) surface potassium decreased benzene formation (Figure 4.28). It was found that potassium and silicon on the (100) surface reduced the amount of surface carbon that accumulated during the reaction and thereby increased the rate of benzene formation relative to the undoped surface (Figure 4.29). The trends at low pressures are presented in Figure 4.30). In general, potassium suppressed, silicon and phosphorus enhanced, and sulfur and chlorine left unchanged the benzene yield. In the presence of sulfur and chlorine the decomposition of acetylene and formation of ethylene were greatly suppressed in UHV. Sulfur-doped Pd(111) was a very selective catalyst for benzene formation from acetylene.

4.3 Discussion

A large amount of data has been presented which studied the effect of surface additives on small molecule bonding. From these results it can be seen that the additives exhibit varying and interesting structure-sensitive behavior. In this section the implications of these results to the fundamental understanding of the interaction of surface additives and their effect on surface bonding and catalytic activity are discussed.

4.3.1 Palladium - Additive Bonding

The strength of the palladium - additive surface bonds varied significantly. Sodium, chlorine and potassium formed much weaker bonds (as evidenced by TPD and AES after heating) than silicon, phosphorus and silicon. For the former additives the activation energy of desorption was lower than for silicon which had a lower activation energy for bulk dissolution. Sulfur and phosphorus were thermodynam-

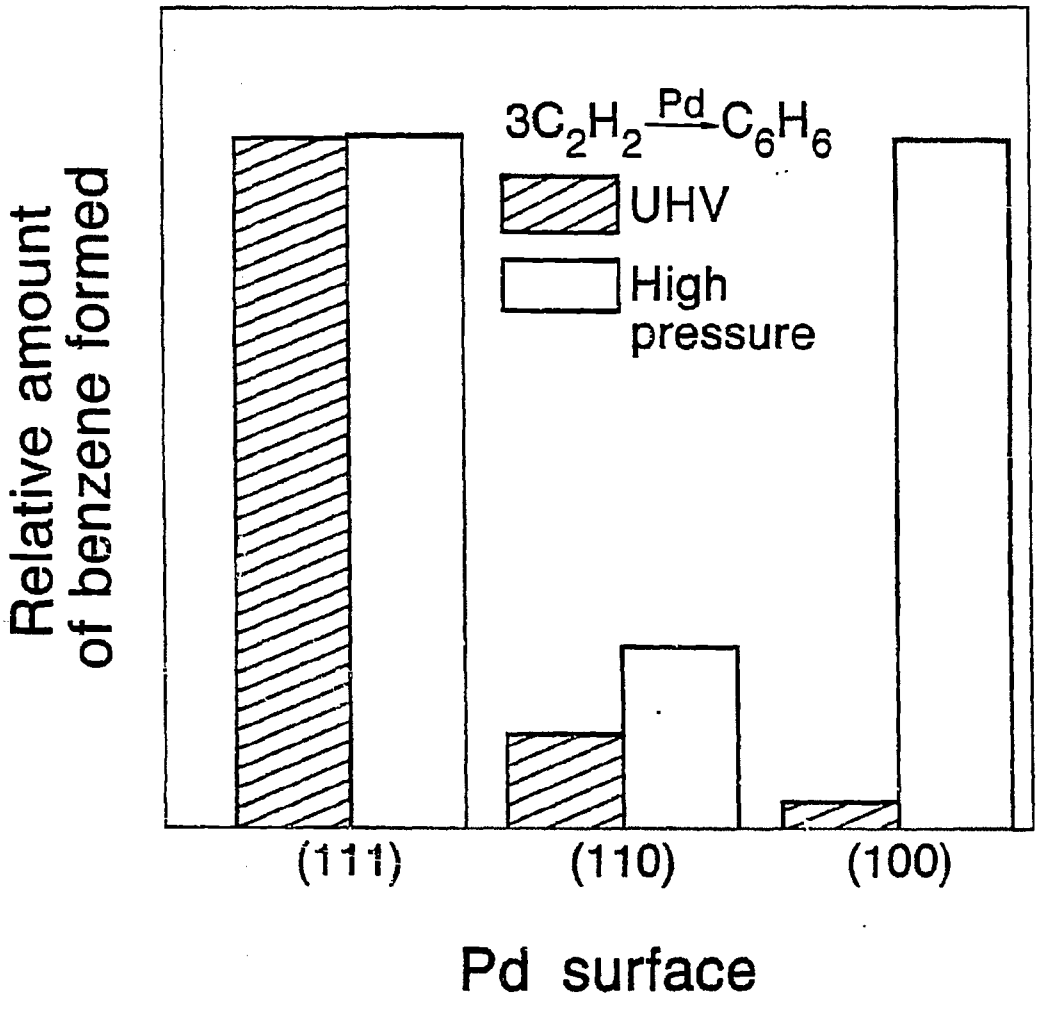

Figure 4.27: This figure shows the structure sensitivity of the acetylene cyclotrimerization reaction in UHV and at atmospheric pressures. In both pressure regimes the reaction is structure sensitive.

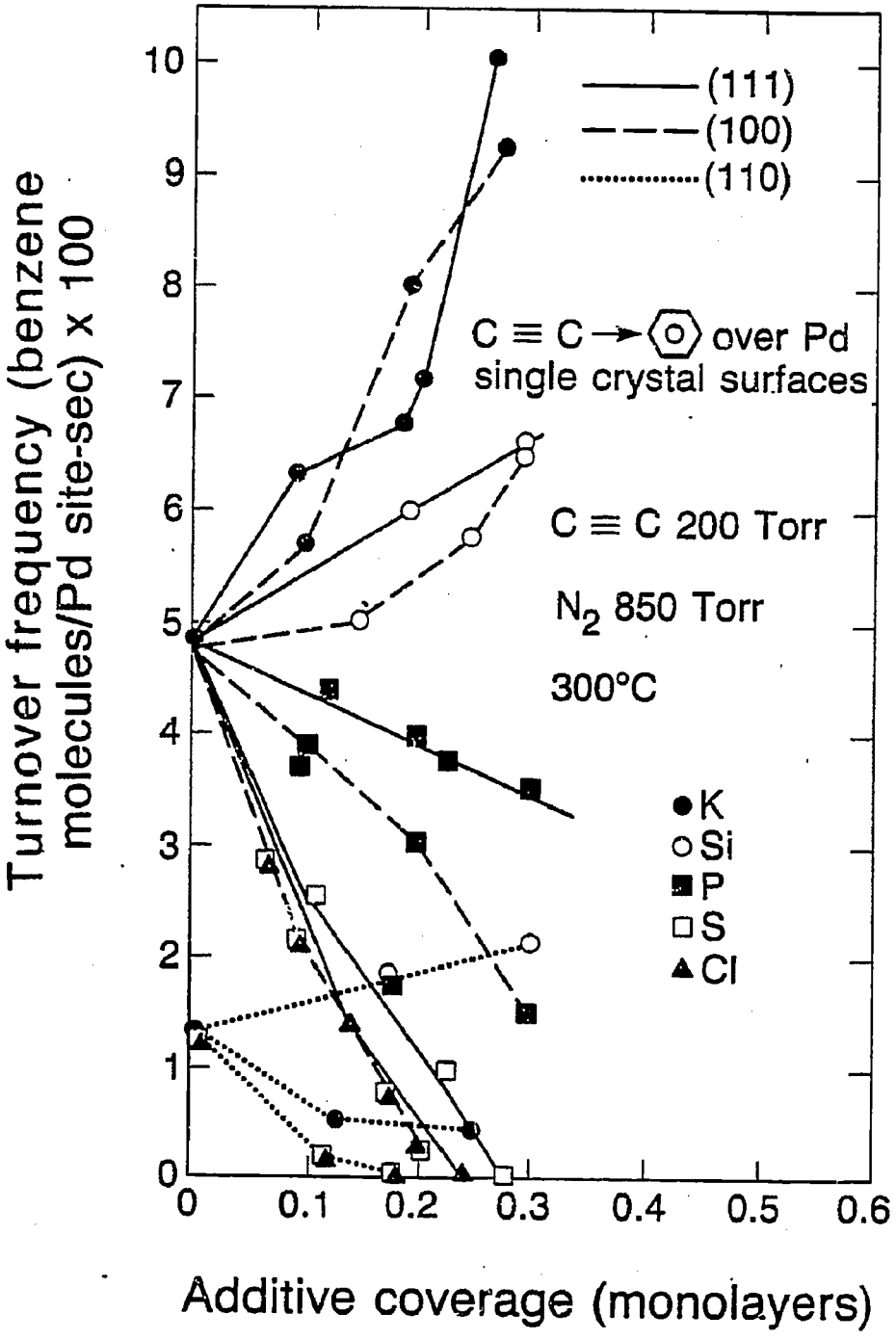

Figure 4.28: Reaction rates of the acetylene cyclotrimerization reaction in the presence of surface additives on the Pd(111), (100) and (110) surfaces at atmospheric pressures. In general, electron-donating additives enhance the rate and electron withdrawing-additives decrease the rate. Potassium on the (110) face is an exception.

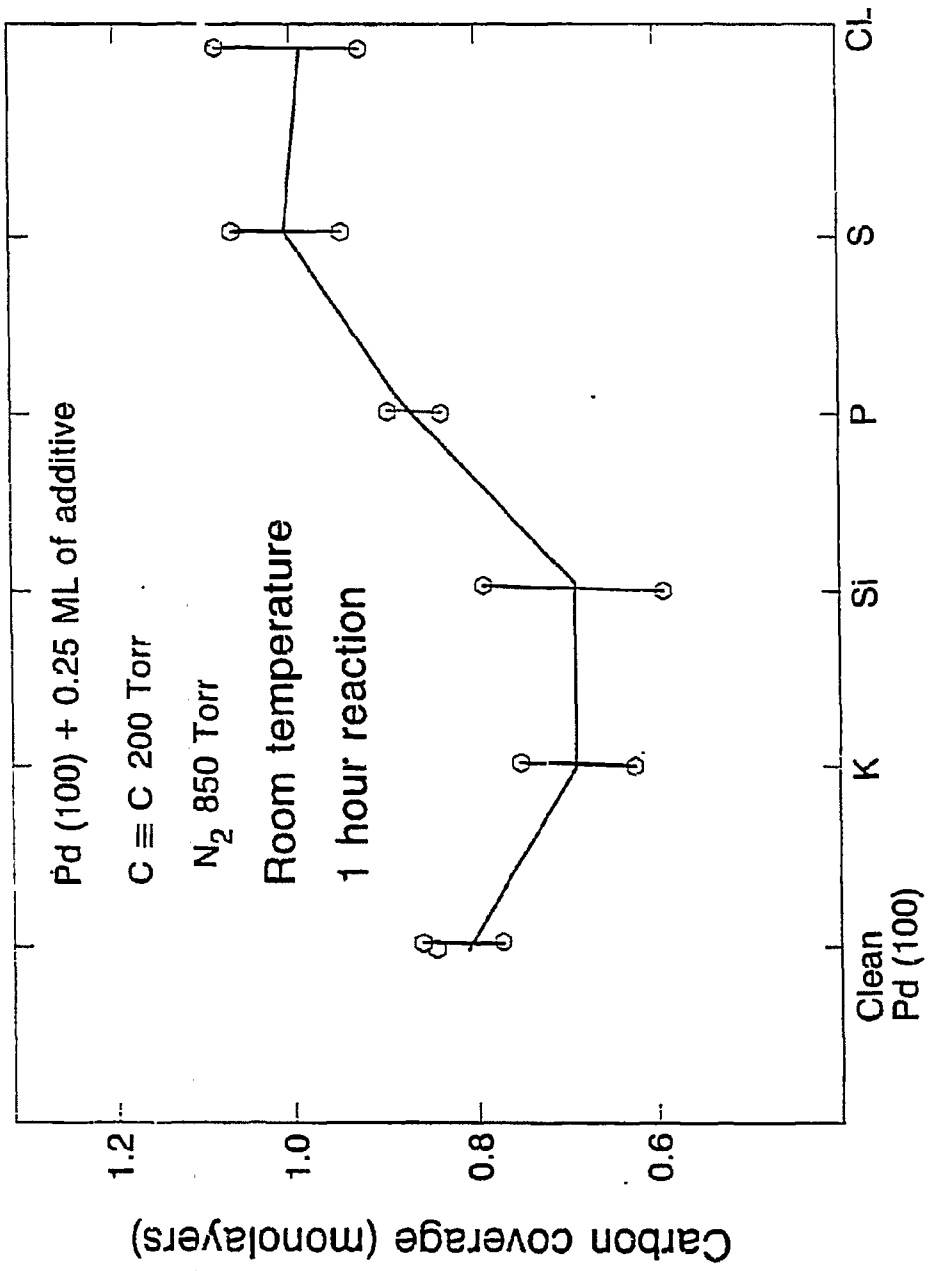

Figure 4.29: This figure shows the relative surface carbon coverage determined by CO titrations after the acetylene cyclotrimerization reaction in the presence of surface additives. Potassium and silicon on the Pd(100) surface reduced the amount of surface carbon buildup during a reaction. These two additives also increased the rate of benzene formation relative to the clean surface.

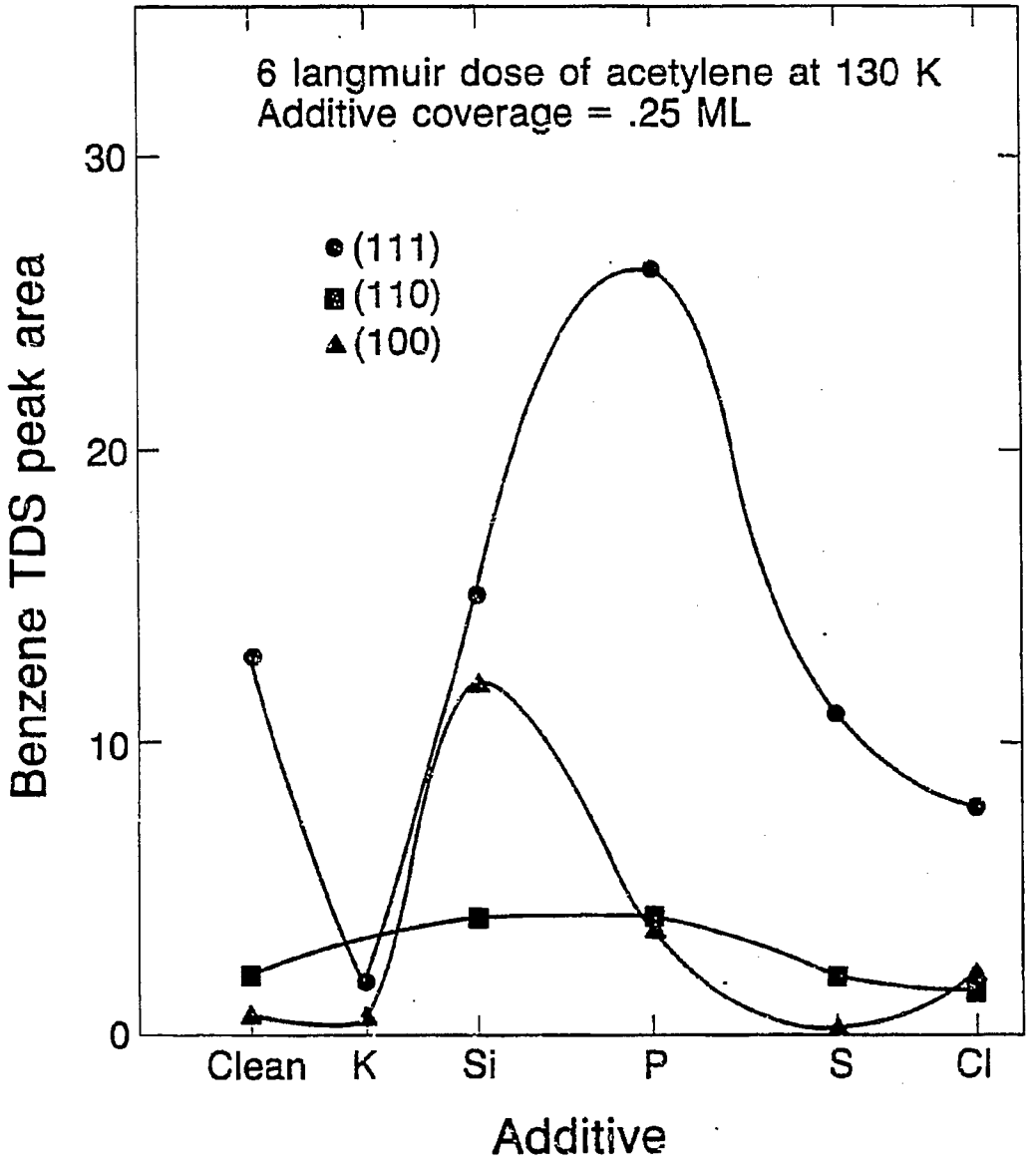

Figure 4.30: The amount of benzene formed in UHV on the additive covered surfaces is shown here. In general, potassium suppressed, silicon and phosphorus enhanced, and silicon and chlorine left unchanged the amount of benzene yield relative to the clean surface.

ically stable on the surface. This trend in the palladium additive bond strength correlates well to palladium complexes and bulk compounds. For example, $PdCl_2$ dissociates almost 400K lower than than PdS [16,17]. Also, palladium silicides are a well known class of bulk compounds.

The LEED work on these additives suggest that they are bound to the metal in high coordination sites: 3- or 4-fold hollow (each additive is bound to three of four palladium atoms). Surface compounds, due to their unique environment and different thermodynamic driving forces (minimizing surface free energy), have no direct analogies in bulk phase diagrams and have different coordination configurations than complexes. This makes it difficult to draw structural or stereochemical correlations. Studies have found potassium to be uniformly dispersed on metal surfaces [18,19] (except at multilayer coverages), whereas sulfur and chlorine form ordered islands at low coverages [20].

On the Pd(100) surface additives linearly change the work function. Potassium, silicon and phosphorus decreased the work function, indicating donation of electron density to the surface, whereas sulfur and chlorine (not pictured) increased the work function, implying withdrawal of electron density. These trends correspond to changes in work function for the Cl/Pd and K/Fe systems [9,10,21]. The work function changes observed correlate to the differences in Pauling electronegativities between the additives and palladium. Potassium (0.82) and silicon (1.9) are more electropositive than palladium (2.2) and donate electron density to the metal, decreasing the work function. Sulfur (2.6) and chlorine (3.2) are more electronegative, thus withdrawing electron density, thereby increasing the work function. Phosphorus (2.19) is essentially electroneutral with respect to palladium, but measurements indicate that it decreases the work function slightly. These changes clearly indicate that there is an electronic interaction between the additives and palladium.

4.3.2 CO Bonding on Clean Palladium

In recent years, many studies have investigated the adsorption of CO on clean palladium single crystals and foils using many techniques including LEED, EELS and IRRAS (infrared reflection absorption spectroscopy) [22,23,24,25,26,27]. The molecular simplicity and strong dipole has made this molecule an excellent surface sensitive probe. It is generally accepted that CO on most palladium surfaces occupies a bridge bonding site, that is, the carbon is bound to two palladium atoms. This is suggested by looking at the CO stretching frequency with either IR or EELS. The correlation between frequency and binding sites are classified as: > 2000 cm^{-1} - top site, 1700 - 2000 cm^{-1} - bridged and < 1700 cm^{-1} three or four fold hollow. On the clean Pd(111) surface a CO stretching frequency at 1835 cm^{-1} was found which is similar to the value of 1823 cm^{-1} reported by Bradshaw and Hoffman [28,29]. CO shows reversible molecular adsorption on all palladium surfaces. After TPD no evidence of carbon buildup was seen. Also, at high CO pressures (in the CO + H_2 reaction, 1:2, 300 psi total pressure, (see Chapter 3) there was no carbon overlayer buildup. CO has been reported to order on all three low Miller index planes used in this research. On the (111) surface a $(\sqrt{3}\times\sqrt{3})R30°$ forms, on the (100) face a (4 × 2)R45° forms and on the (110) face a c(2 × 2) at low coverages and a (4 × 2) at high coverages forms. High concentrations of CO on the surface have also been reported to change the bonding as evidenced by IR and heats of adsorption. This work and work by others found a 10 kcal/mol shift in heats of desorption between low and high CO surface coverages. Also the CO stretching frequency shifts from $\sim$ 1800 cm^{-1} to 1950 cm^{-1} . Palazov *et al.* have studied palladium on silica and proposed that at high CO coverages a linear top site CO binding site evolves [30]. Theoretical calculations by Batra and Bagus have suggested that higher CO concentrations on the surface lead to direct intermolecular repulsion and reduction of backbonding via competition from

neighbors [31].

Differences in CO bonding sites and the effect of surface additives can be better understood by seeing how CO bonds to metals. Figure 4.31 shows a molecular orbital diagram of CO and a metal atom. According to the Byholder model, CO binds to the metal 4d orbital through its 5σ molecular orbital to form a sigma bond [32,33]. The CO $2\pi^*$ antibonding orbitals also bond to metal 4d orbitals to form what is commonly referred to as the back-bonding or pi bond. The strength of the M-CO bond is determined by electron density in these bonds.

4.3.3 The Effect of Additives on CO Bonding

The extensive amounts of literature on the CO/Pd system shows that metal-CO bonding is well understood. Using this knowledge base we can use CO as a probe to better understand the effect of surface modifiers. Table 4.2 summarizes the changes in CO bonding induced by surface additives on the palladium (111), (110) and (100) faces.

The two generally accepted forms of additive interactions on surfaces are either electronic or structural. In the structural or site blocking interaction the additive physically hinders the adsorption of other molecules, whereas with an electronic interaction the charge density on the surface is altered to affect chemical bonding of molecules to the surface. Table 4.3 and Table 4.4 summarize the experimental and theoretical work by other groups which have studied the influence of additives. From these tables it can be seen that most groups have proposed that the additives either sterically or electronically change the chemisorption properties of the metal. However as will be discussed, it is necessary to invoke both types of interactions to completely explain the effect of surface additives on bonding and catalytic reactions. Surface additives form strong bonds with palladium as shown earlier. These additives block sites as evidenced by the decrease in CO chemisorption as

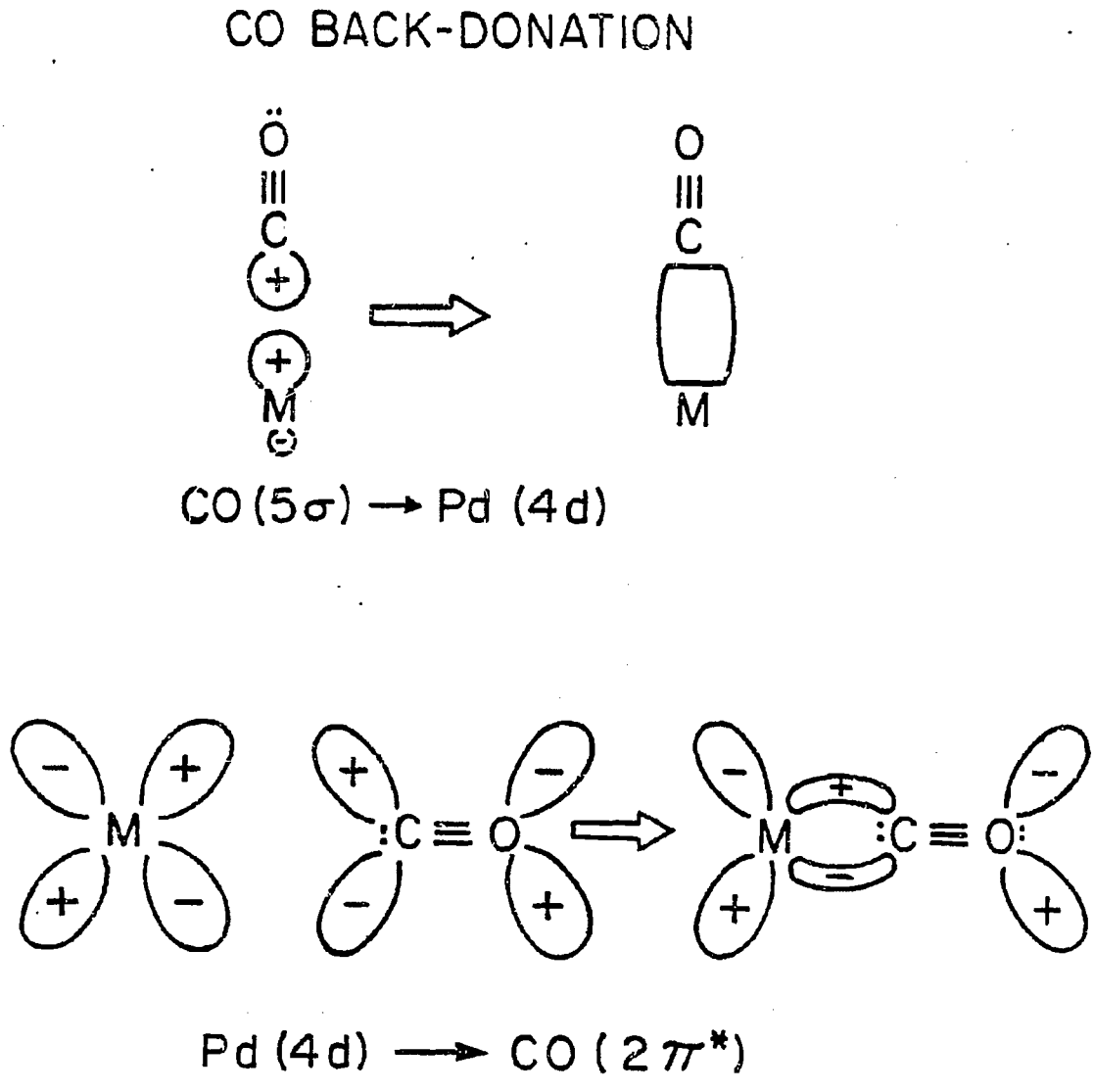

Figure 4.31: This figure shown a molecular orbital diagram of CO and a metal atom. The CO binds to the metal 4d orbitals through its 5σ molecular orbital to form a sigma bond, and through its $2\pi^*$ antibonding orbital to form what is commonly referred to as the back-bonding or pi bond.

Addit.	(111)	(100)	(110)
Clean	480K maximum, sharp 150K (sh) med. cover. 320K, high coverages	470K max. 420K (390K sh) (med) 420K,360K high cov.	450K Maximum Broad peak 430K at med. cover. 430K, 370K & 270K at high cover.
K, Na	Increase temp., shift. not much change in broadness	Increase Temp. new peak at higher Θ_K	Decrease Temp., new sites, broadening
Si	Gradual shift	Gradual shift, no broadening	Gradual shift, no broadening
P	20K shift followed by new peak at Θ_P=.35	Shift of 80K at Θ_P=.26 broadening poss. indicative of two peaks	Gradual shift 50K atΘ_P=.5
S	Shift 50K, new peak at Θ_S=.43	New peaks	Gradual shift Θ_S=.4 then new peak
Cl	Low cover. new peaks	Shifts - higher addit. cover. have larger shift	Gradual shift then new peak

Table 4.2: Summary of the CO TPD shifts on the additive-covered palladium faces

Substrate	Additive	Conclusions	Reference
Ni(100)	S	steric, local interactions	Gland [34]
Ni(100)	Cl, S, P	electronegativity	Kiskinova [35]
Ru(001)	Na	molec. reorientation of CO	Netzer [26]
Pd(110)	Na	LEED, surf. reconstruc.	Barnes *et al.* [6]
Ni, Pt, Pd (110)	Cl	LEED, TPD, $\Delta\Phi$	Erley [10]
Pd, Pt (111)	Cl	LEED, TPD, $\Delta\Phi$	Erley [9]
Pd(110)	S	LEED Equilibrium Configuration	Peralta [8] Madey [36]
Pd Foil	P	Pd-P compound	Sundram [37]
Pd(111),(110),(100)	K,Na,Si, P,S, Cl	Convolution of Electronic and Steric Interac.	This study

Table 4.3: Summary of some previous experimental studies of the interaction of additives on selected transition metals

a function of additive coverage. They change the bonding of CO to the surface as shown by changes in desorption temperature, formation of new CO desorption peaks and changes in stretching frequencies (determined by EELS). Since bonding involves sharing of electrons, the additives can also modify the distribution of surface electrons available for bonding with CO or any other adsorbate, in some or all of the possible binding sites.

The additives change the surface electron concentration (seen by $\Delta\Phi$) by withdrawing or donating electron density. On the (111) and (100) surfaces increasing the surface coverage of electronegative additives (Si, P, S, Cl) decrease the desorp-

Substrate	Additive	Conclusions	Reference
Trans. Metals	alkali,P,S,Cl,O	electrostatic interactions	Lang [38]
Trans. Metals	electronegative & electropositive	electrostatic interactions discuss structure sensitivity	Norskov [39]
Trans. Metals	alkali	electronic charge transfer	Albano [40]
Fe(100)	S,C,O	direct interaction between CO and additive	Benziger [41]
Ni(001)	S	electronic and geometric	Pendry [42]
Rh(001)	P,S,Cl,Li	electronic	Feibelman [43]

Table 4.4: Summary of some previous theoretical studies of the interaction of additives on selected transition metals

tion temperature of CO whereas electropositive additives (K, Na) increase the CO desorption temperature. Figure 4.32 shows the activation energies of desorption (calculated from the desorption temperature using the Redhead method [44]) of CO from additive covered Pd(111) and (110). Generally, the more electronegative an additive the larger is the decrease in the desorption temperature at a given coverage. From the Blyholder [32,33] CO bonding model discussed earlier, it can be seen that an electronegative adatom would withdraw electron density from the metal, thereby decreasing the 4d - $2\pi^*$ orbital density and weaken the metal - CO bond. Therefore, a lower desorption temperature corresponds to a weaker M-CO bond and a higher desorption temperature corresponds to a stronger M-CO bond. The rate of acetylene cyclotrimerization at high pressures also follows the general trend that more electronegative additives enhance the benzene yield. These promoting additives limit the decomposition or rate of polyacetylene formation (which block active sites) on the catalyst surface. Previous studies have

found that electron withdrawing additives enhance the polymerization process by acidifying the metal surface [45].

There are many changes in bonding and catalytic activity of the additive-covered palladium surfaces which cannot be explained by a simple electron density arguement. Some examples are the increase on the CO desorption temperature and decrease in the acetylene cyclotrimerization rate on the potassium- and sodium-covered (110) surface in contrast to the other surfaces, the presence of new CO binding sites which grow in with increasing additive coverage (P on Pd(111)) and the differences in CO bonding for the same additive on different crystal faces.

Therefore, another form of additive interaction that needs to be considered is structural. Changes in surface structure or ensemble size (number of palladium atoms clustered together without additive) induces the largest shifts. The most striking example is with sodium- or potassium-doped surfaces. On the (110) surface, which undergoes restructuring [6], the CO desorption maximum shifts to lower temperatures, whereas on the (111) and (100) surface the desorption maximum shifts to higher temperatures. By charge transfer arguments, the desorption temperature should shift to higher temperatures on all three surfaces. Change in work function measurements show that on the (110) surface potassium does not donate as much electron density as on the (100) surface. (Figure 4.33). A reason for this difference might be that the more open surfaces have Fermi levels [46] closer to the potassium fermi level and that charge transfer is minimized [40]. Netzer *et al.* found for low sodium coverages and saturation CO coverages on Ru(001) that a fraction of the CO molecules undergo changes in bonding configuration - from linear to inclined [47]. The rearrangement of the surface and the minimal differences in electronic interaction of alkali metals on the three low Miller index planes suggest that a major determinant of CO bonding is structural.

This ensemble, or structure effect, is also evident on surfaces which do not

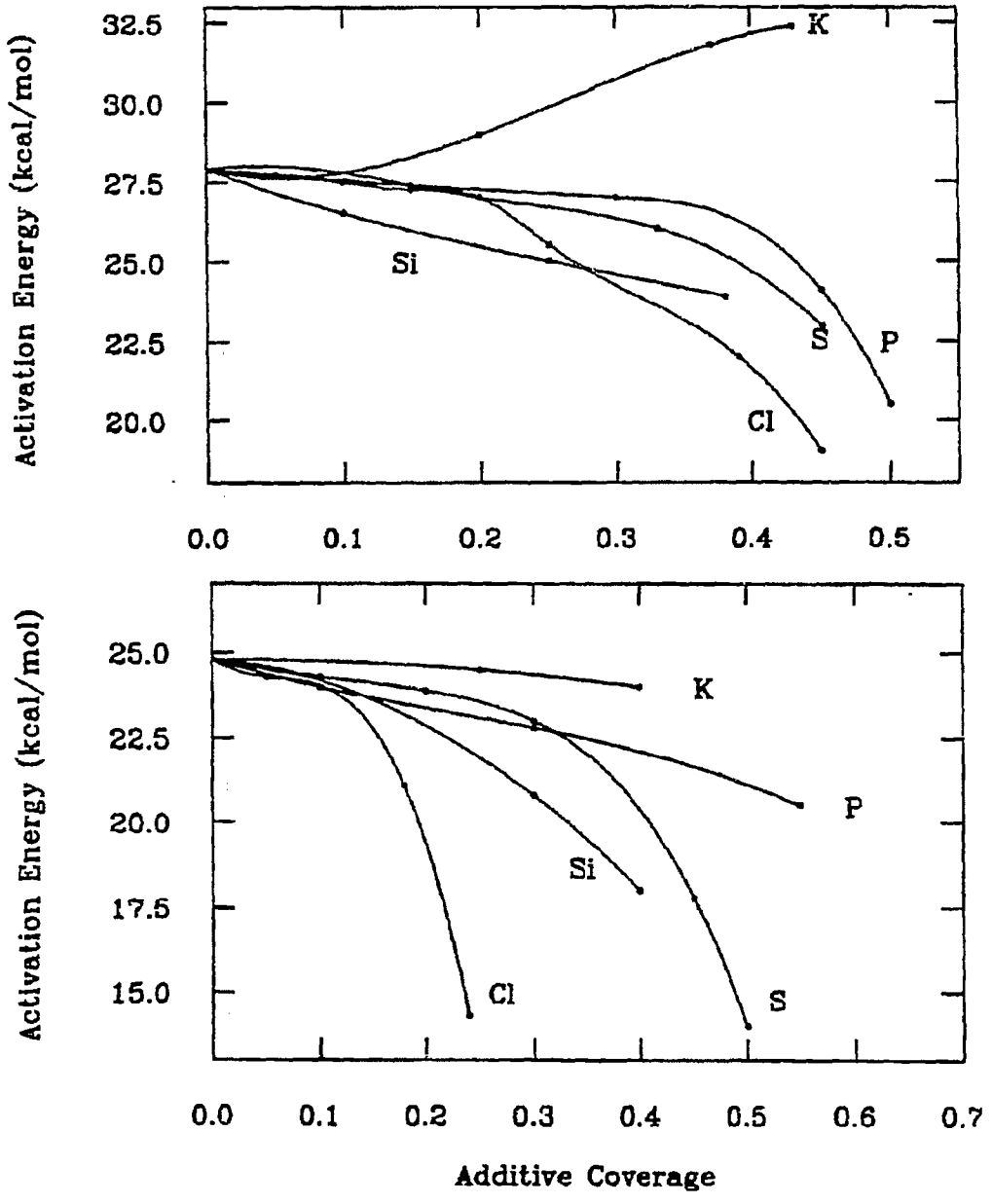

Figure 4.32: These two graphs show the activation energy of desorption of CO from additive covered Pd(111) and (110). In general, the more electronegative an additive, the larger the decrease in desorption temperature at a given coverage. The sharp changes in slope at higher coverages are due to the population of a new low temperature binding site.

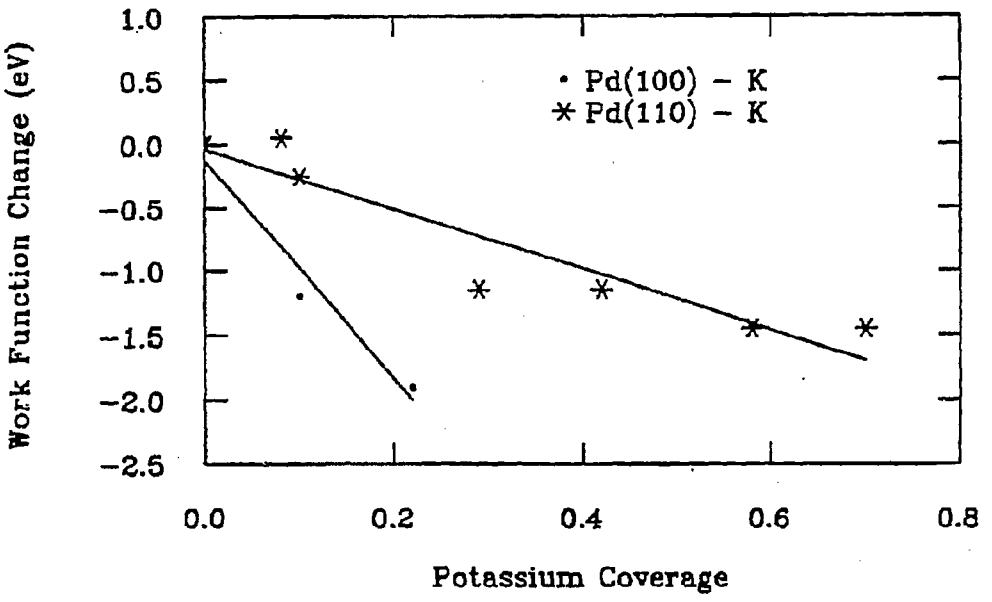

Figure 4.33: This figure shows the changes in work function for the Pd(110) and (100) surfaces as a function of increasing potassium coverage. On the more open (110) surface, potassium does not lower the work function as much as on the (100) surface.

undergo surface reconstruction. As the additive coverage increases, the number of large palladium clusters decreases, favoring less stable bonding configurations for the CO. These shifts have been observed in a Ag-Pd alloy by Soma-Noto and Sahtler [48]. They found a maximum in the IR bands of linearly bound species on a 70% - Pd alloy with a constant decrease in bridge bound species. The linear bound species had desorption energies $\sim$ 15 kcal/mol lower than the bridge bound species. On numerous modified palladium systems, a new low temperature CO desorption peak grows in at additive coverages between Θ= .25 - .45 (Pd(111) - S, P, Cl; Pd(110) - S, Cl). At low CO exposures, it is possible that the additives force the CO into binding configurations accessible only under high CO exposures where there is CO crowding. Previous studies on Pd single crystals [49] indicate that CO desorption is a first order process, and that the desorption energy is coverage dependent due to CO - CO interactions. Therefore the shift in peak maximum at higher additive coverages could be attributed to these interactions. It does not seem that this perturbation is a major factor at low CO exposures. In most cases the desorption maximum shifts in differing amount relative to the clean surface which is dosed with higher CO exposures.

Another factor supporting a structural interaction of ensemble size effects is the cyclotrimerization of acetylene to form benzene. On the potassium-doped (110) surface benzene formation is hindered relative to the clean surface, in contrast to the (111) and (100) surfaces where the rate is enhanced by a factor of five. To form benzene, three acetylene molecules must be able to bond in close proximity to each other. On the (110) restructured surface, the palladium ensemble size has diminished to a point where the reaction cannot take place.

A fourth factor favoring the structure argument is the structure sensitivity in the CO desorption shift for the additives. Phosphorus on the three surfaces induces vastly different CO binding states. On the (111) surface at low coverages

there is a gradual decrease ($\sim$ 20°) in the desorption maximum followed by the appearance of a new binding state (50° lower) at phosphorus coverages above Θ = .35, whereas on the (110) surface there is a gradual decrease in the CO maximum with increasing phosphorus coverage. If the CO - metal - P interaction were purely electronic, similar trends in the CO trace would be expected (i.e. only shifts, or new CO TPD peaks forming on both surfaces) with only the magnitude being affected by the metal - phosphorus bonding orbital overlap.

The CO TPD traces do not undergo any shape changes or broadening as a function of additive coverage. This implies that the energies of the CO binding sites are relatively homogeneous at most additive coverages. After the CO molecules adsorb on the surface they must diffuse to a low energy binding site on the surface. On the surface additive systems where new peaks are resolvable, more than one binding site is energetically favorable and the activation barrier for diffusion is high. Arias *et al.*, using metastable quenching spectroscopy, found that at low CO exposures the CO molecules are adsorbed near potassium and at high potassium coverages the CO molecules lie flat on the surface or very much tilted from the surface normal [50]. The presence of only limited sites is supported by the EELS data for the Pd(111) - S surface, which shows two different binding sites for CO, a bridged species intense at low sulfur coverages and a tilted species which increases in intensity with increasing sulfur coverage. These two species have been assigned to the high temperature CO desorption (bridged) and low temperature CO desorption (tilted). The tilting may be due to either a steric interaction between the additive and CO or an electronic 'bonding' between the CO π orbitals and the additive.

Another effect these surface additives exhibit is the purely steric or site blocking effect. At high CO exposures the amount of CO desorbing decreases with increasing additive coverage.

Figure 4.34 shows some of the possible bonding configurations of CO in the presence of surface additives which correlate to the experimental results and interpretations. As seen by these changes in CO chemisorption, the additives modify CO bonding both structurally and electronically.

In the literature there has been extensive study of the long range vs. short range interactions of surface additives [51]. The easiest way to discern these effects is to study the change in CO binding as a function of additive coverage. If long range interactions are dominant there would be a continuous variation in the CO binding energy and broad peaks would be detected, since the additive's influence would decay over numerous CO binding sites. If short range interactions are dominant, then only the nearest CO binding states would be effected and the remaining sites would remain unperturbed. In this case CO might be expected to exhibit discreet binding states. Since only a few of the CO TPD traces showed any broadening, and in some cases this broadening was due to multiple sites, it can be said that the additives exhibit only a short range effect.

4.3.4 Effect of Additives on Hydrogen Bonding

The effect of the surface additives on hydrogen chemisorption on the palladium single crystals is very different than that seen for CO. The amount of hydrogen desorbing decreased as the additive concentration increased without changing the desorption temperature or activation energy of desorption. On all three surfaces. phosphorus, sulfur and chlorine, in that order, decreased the amount of hydrogen bound to the surface at a given coverage. Since there was no change in the desorption temperature this decrease can be attributed to site blocking by the additive. However, chlorine, which for a given coverage had the largest effect has the smallest ionic radius. Similar desorption temperatures for hydrogen from the clean surface were seen by other groups [4,52.35].

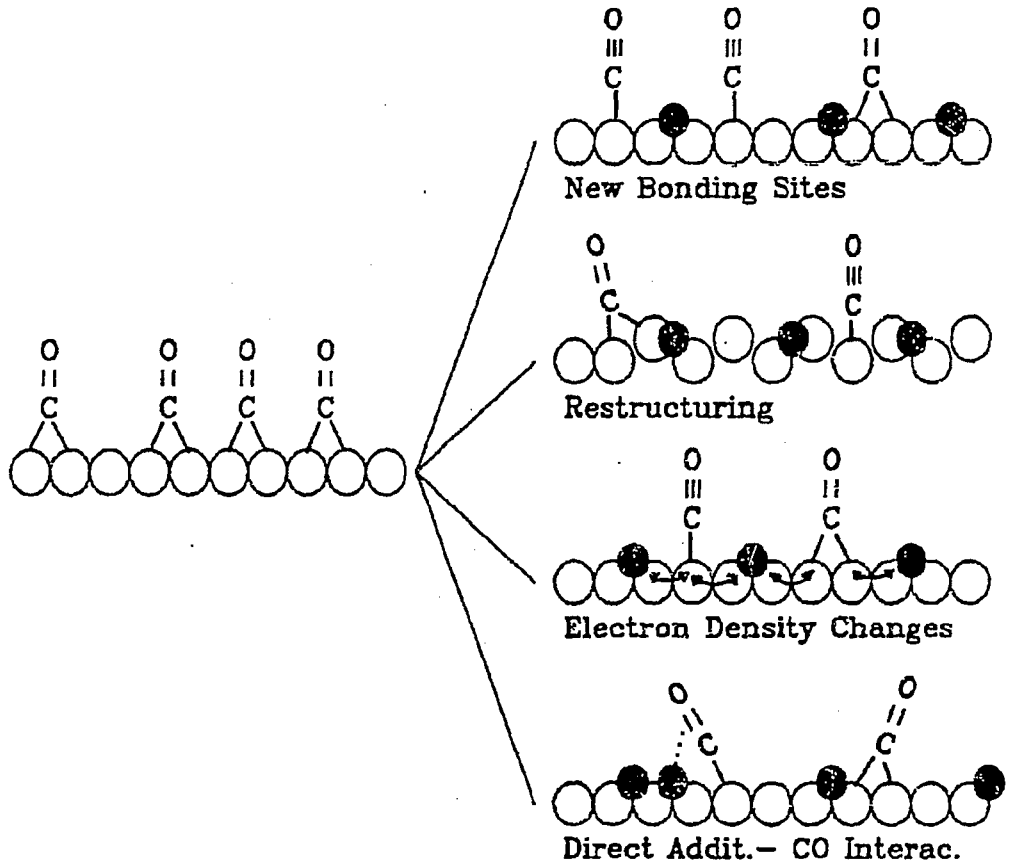

Figure 4.34: This figure shows some of the possible bonding configurations of CO in the presence of surface additives. These additives both structurally and electronically modify the bonding relative to the clean surface.

Hydrogen dissociatively adsorbs on palladium and it easily dissolves into the bulk [53,54,55]. At room temperature the metal has the unusual property of absorbing 900 times its own volume of hydrogen, possibly forming Pd_2H. Most likely the additives affect the adsorption process rather than the desorption process where the rate determining step is hydrogen recombination. Hydrogen also bonds in the four fold sites that are preferred by the additives. The additives lower the sticking coefficient of hydrogen, with the more electronegative additives having a larger effect. This decrease in the sticking coefficient is due an activated adsorption of hydrogen on the surface in a process that involves dissociation.

4.3.5 Palladium - Silicon

In studying the effects of the additives on work function changes, and on CO and H_2 bonding, K, P, S, and Cl followed each other, whereas silicon exhibited very unique and different effects. For instance, in hydrogen chemisorption on the (100) surface there was an increase in the hydrogen chemisorption relative to the clean surface while the other additives decreased the amount of hydrogen bonding. In CO bonding, silicon on all three surfaces gradually shifted the desorption maximum without forming a new peak. The other additives produced more varying features. Also, the decrease in the activation energy of desorption did not follow in the trends established by the other additives based on electronegativities. With silicon, unlike any of the other additives, annealing the surface, changed the work function by .75 eV (closer to clean Pd(100)), while only slightly decreasing the surface concentration as measured by AES. All this evidence of silicon's unique behavior suggests that silicon forms a palladium silicide in the near-surface region. Surface compound formation has been proposed on other systems [21,56,57,58,59,60,61,62,63,64]. Pd_xSi_y compounds do exist and are very stable [65]. The surface compound exhibits very different chemistry than a surface

only decorated with an additive.

4.4 Conclusions

The following list of points summarize the results in studying the effect of additives on the surface chemistry of palladium single crystals ((111),(100) and (110)).

- The Pd - Additive bond strength ordering is Na < Cl < K << Si < P < S.
- The additives modify CO bonding through the convolution of both electronic and structural interactions with the surface and CO.
- The additives change only the relative sticking coefficient of hydrogen to the surface and do not change the desorption temperature.
- Palladium can form a surface palladium silicide which has different bonding properties than would be expected if silicon followed in the trends established by the other additives.

References

[1] H. P. Bonzel. *J. Vac. Sci. Tech* **A2** (1984) 866.

[2] D. W. Goodman. *J. Vac. Sci. Tech.* **20** (1982) 522.

[3] G. Ertl. *Catalysis, Science & Technology (Vol. 4).* Springer, 1983.

[4] H. Conrad, G. Ertl, and E. E. Latta. *Surf. Sci.* **41** (1974) 435.

[5] J. C. Tracey and P. W. Palmberg. *J. Chem. Phys.* **51** (1969) 4852.

[6] C. J. Barnes, M. Q. Ding, M. Lindroos, R. D. Diehl, and D. A. King. *Surf. Sci.* **162** (1985) 59.

[7] W. Berndt, R. Hora, and M. Scheftler. *Surf. Sci.* **117** (1982) 188.

[8] L. Perlata, Y. Berthier, and M. Huber. *Surf. Sci.* **104** (1981) 435.

[9] W. Erley. *Surf. Sci.* **94** (1980) 281.

[10] W. Erley. *Surf. Sci.* **114** (1982) 47.

[11] Y. Nakamoto. *Infrared & Raman Spectra of Inorganic and Coordination Compounds.* Wiley, 1978.

[12] I. A. Oxton. *J. Molec. Struct.* **78** (1982) 77.

[13] D. M. Adams and I. D. Taylor. *J. Chem. Soc. Faraday Trans.* **78** (1982) 1551.

[14] M. A. Logan, T. G. Rucker, T. M. Gentle, E. L. Muetterties, and G. A. Somorjai. *J. Phys. Chem.* **90** (1986) 2709.

[15] T. G. Rucker, M. A. Logan, T. M. Gentle, E. L. Muetterties, and G. A. Somorjai. *J. Phys. Chem.* **90** (1986) 2703.

[16] F. Weibke and J. Laar. *Z. Anorg. Chem.* **224** (1935) 49.

[17] J. Krustinsons. *Z. Elecktrochem.* 44 (1938) 537.

[18] G. Pirug, H. P. Bonzel, and G. Broden. *Surf. Sci.* **122** (1982) 1.

[19] E. L. Garfunkel and G. A. Somorjai. *Surf. Sci.* **115** (1982) 441.

[20] G. A. Somorjai. *Chemistry in Two Dimensions.* Cornell University Press, Ithaca, New York, 1981.

[21] G. Ertl and J. Kuppers. *Low Energy Electrons and Surface Chemistry.* Verlag Chemie, 1974.

[22] R. P. Eischens and W. A. Pliskin. *Advan. Catalysis* **10** (1958) 1.

[23] J. P. Biberian and M. A. van Hove. *Surf. Sci.* **118** (1982) 443.

[24] A. Ortega, F. M. Hoffman, and A. M. Bradshaw. *Surf. Sci.* **119** (1982) 79.

[25] H. Conrad, G. Ertl, J. Koch, and E. E. Latta. *Surf. Sci.* **43** (1974) 462.

[26] F. P. Netzer and M. M. El Gomati. *Surf. Sci.* **124** (1983) 26.

[27] S. Sung and R. Hoffmann. *J. Amer. Chem. Soc.* **107** (1985) 578.

[28] A. M. Bradshaw and F. Hoffmann. *Surf. Sci.* **52** (1975) 449.

[29] A. M. Bradshaw and J. Pritchard. *Proc. Roy. Soc. (London)* **A316** (1970) 169.

[30] F. Palazov. *J. Catalysis* **74** (1982) 44.

[31] I. P. Batra and P. S. Bagus. *Solid State Commun.* **16** (1975) 1097.

[32] G. Blyholder. *J. Phys. Chem.* **68** (1964) 2772.

[33] G. Blyholder. *J. Vac. Sci. Tech.* **11** (1974) 865.

[34] J. L. Gland, R. J. Madix, R. W. McCabe, and C. DeMaggio. *Surf. Sci.* **143** (1984) 46.

[35] M. Kiskinova, G. Bliznakov, and L. Surnev. *Surf. Sci.* **94** (1980) 169.

[36] T. Madey, J. T. Yates, A. M. Bradshaw Jr., and F. M. Hoffmann. *Surf. Sci.* **89** (1979) 370.

[37] V. S. Sundaram, S. P. da Cunha, and R. Landers. *Surf. Sci.* **119** (1982) L383.

[38] N. D. Lang, S. Holloway, and J. K. Norskov. *Surf. Sci.* **150** (1985) 24.

[39] J. K. Norskov, S. Holloway, and N. D. Lang. *Surf. Sci.* **137** (1984) 65.

[40] E. V. Albano. *Surf. Sci.* **141** (1984) 191.

[41] J. Benziger and R. J. Madix. *Surf. Sci.* **94** (1980) 119.

[42] J. M. Maclaren and J. B. Pendry. To be published.

[43] P. J. Feibelman and D. R. Hamann. *Surf. Sci.* **149** (1985) 48.

[44] P. A. Redhead. *Vacuum* **12** (1962) 203.

[45] C. N. Satterfield. *Heterogeneous Catalysis in Practice.* McGraw-Hill, 1980.

[46] R. Smoluchowski. *Phys. Rev.* **60** (1941) 661.

[47] F. P. Netzer, D. L. Doering, and T. E. Madey. *Surf. Sci.* **143** (1984) L363.

[48] Y. Soma-noto and W. M. H. Sachtler. *J. Catalysis* **32** (1974) 315.

[49] P. Ladas, H. Poppa, and M. Boudar. *Surf. Sci.* **102** (1981) 151.

[50] J. Arias, J. Lee, J. Dunaway, R. Martin, and H. Metiu. *Surf. Sci.* **159** (1985) L433.

[51] K. Markert and K. Wandelt. *Surf. Sci.* **159** (1985) 24.

[52] M. G. Cattania, V. Penka, R. J. Behm, K. Christmann, and G. Ertl. *Surf. Sci.* **126** (1983) 382.

[53] R. J. Behm, K. Christmann, and G. Ertl. *Surf. Sci.* **99** (1980) 320.

[54] J. P. Muscat and D. M. Newns. *Surf. Sci.* **80** (1979) 189.

[55] F. A. Lewis. *The Palladium - Hydrogen System.* Academic Press, 1967.

[56] E. Baner, H. Poppa, and V. Viswanath. *Surf. Sci.* **92** (1980) 53.

[57] E. Baner, H. Poppa, and V. Viswanath. *Surf. Sci.* **93** (1980) 407.

[58] H. M. Kramer and E. Bauer. *Surf. Sci.* **92** (1980) 53.

[59] H. M. Kramer and E. Bauer. *Surf. Sci.* **93** (1980) 407.

[60] Y. P. Zingermann and V. A. Ishchuk. *Fiz. Tver. Tela.* **9** (1967) 2529.

[61] P. H. Holloway and J. B. Hudson. *Surf. Sci.* **43** (1974) 123.

[62] J. E. Denath and T. N. Rhodin. *Surf. Sci.* **45** (1974) 249.

[63] K. Akimoto, Y. Sakisaka, and M. Onichi. *Surf. Sci.* **82** (1979) 349.

[64] C. A. Papageorgopoulos and C. A. Chen. *Surf. Sci.* **52** (1975) 40.

[65] *Handbook of Chemistry and Physics.* C. R. C. Press, 1983.

Chapter 5

PEROVSKITES

5.1 Introduction

Perovskite oxides are a class of compounds which are important in many areas of science and technology due to their physical properties, which include ferroelectricity, piezoelectricity, pyroelectricity, magnetism, high temperature superconductivity and electrooptic effects. This class of compounds has the general formula ABO_3, where A is a large ion with a filled d shell and B is a smaller transition metal. Figure 5.1 shows the crystal structure of a perovskite with the $CaTiO_3$ structure. Tetragonal and rhombohedral distortions are not uncommon, and it has been shown that small changes in structure and composition result in large changes in the electronic properties [1,2].

Only in the last sixteen years has there been any interest in these materials as catalysts [3]. Most of the catalytic research has centered on developing stable and active catalysts for the treatment of automobile exhaust in catalytic converters. Cobalt, platinum, ruthenium and manganese type perovskite compounds have shown activity in the oxidation of nitric oxide [4]. However their low conversions and sensitivity to sulfur poisoning limited their application in this field.

Concurrently there has been interest in producing two carbon oxygenate molecules from carbon monoxide and hydrogen such as ethanol, ethylene glycol and

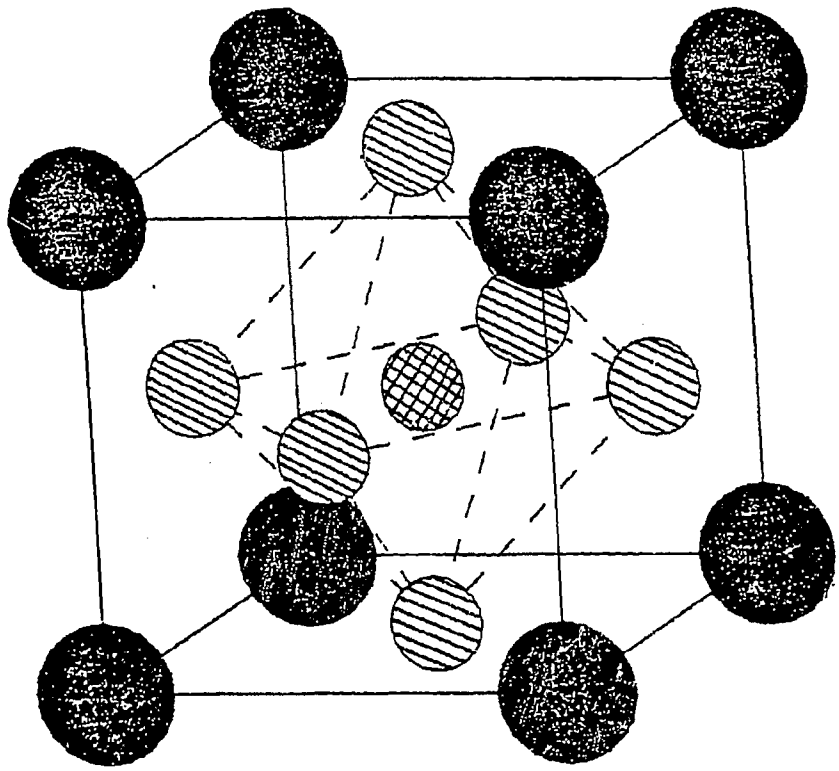

Figure 5.1: Crystal structure of perovskite compounds.

acetic acid. Supported rhodium catalysts have shown high activity in forming these molecules but the product distribution is very sensitive to the catalyst preparation [5,6,7,8,9]. It appears that the chemical state of the rhodium varied widely in these different samples. Previous research in our group has centered on modeling these supported rhodium catalysts with low-surface-area well-characterized rhodium single crystals and foils [10,11,12]. These studies found that metallic rhodium is a stable, but average methanation catalyst. Oxidation prior to a reaction activated the foil for ethanol formation but this surface was unstable in the reducing conditions of the CO + H_2 reaction. Under the same conditions rhodium sesquioxide reduced only slightly and lanthanum rhodate did not reduce. Both of these compounds had a relatively high yield of oxygenated (+25%) products.

The possibility that the perovskite structure could stabilize an oxidized form of a metal led us to study this class of compounds in the CO hydrogenation reaction. In this chapter the catalytic activity of perovskite compounds $LaMO_3$ (M = Rh, Cr, Mn, Co and Fe) is reported and compared to the catalytic behavior of the oxidized and reduced metal alone.

5.2 Results and Discussion

5.2.1 Introduction

This section presents and discusses the results obtained in the survey of the lanthanum perovskite compounds $LaMO_3$ (M = Cr, Mn, Co, Rh, and Fe). The powered samples were compressed into a .005 in gold mesh at $\sim$ 25,000 psi. This mesh was then spotwelded to a 1 cm^2 .010 in gold foil which in turn was attached to the manipulator. All reactions were run at 250°C, 2:1 H_2:CO ratio with a total pressure of 300 psi (20 atm).

5.2.2 Catalytic Studies

The catalytic activity of first row transition metals in $LaMO_3$ perovskite structures was studied in the CO hydrogenation reaction. Figure 5.2 shows normalized product distributions for the five samples. In all cases methane is the major product ranging from 95+ mole-percent of the product distribution on $LaCrO_3$ down to 77 mole percent on $LaFeO_3$. Figure 5.3 shows an expanded view of the percentage of C_2, C_3, C_4 and alcohol molecules formed. $LaFeO_3$ produces almost 3 times as much ethane and ethylene as any of the other samples and $LaCrO_3$ is virtually inactive in forming any products other than methane. All the samples to some degree catalyze the formation of C_3 and C_4 hydrocarbons. No larger molecules were detected in the reaction loop. $LaFeO_3$, $LaCoO_3$ and $LaRhO_3$ showed some activity in alcohol formation, primarily methanol.

Table 5.1 summarizes the initial rate of product formation of the lanthanates expressed as molecules formed per site-second. Moving from left to right through the periodic table it can be seen that the rate of product formation increases: $LaCrO_3 > LaMnO_3 > LaFeO_3 > LaCoO_3 \sim LaRhO_3$. The differences in activity are tremendous and span 2 orders of magnitude. This shows that the metal (Cr, Mn, Fe, Co and Rh) both the selectivity and activity of the catalyst. The role of the lanthanum oxide cannot be elucidated from the data, but it might be either a structural support, a promoter providing a mixed catalytic site with the metal, or it may keep the metal in an oxidized state.

From CO chemisorption results, Cr and Mn dissociatively bond CO whereas Co and Rh exhibit CO bonding where there is some dissociation followed by recombination and desorption. Cr and Mn, in general, irreversibly bind hydrocarbons whereas Rh forms weaker bonds which leads to less decomposition [13]. On the samples with lower rates such as $LaCrO_3$ and $LaMnO_3$, a large carbon concentration was detected after the reaction. This suggests that during the reaction the

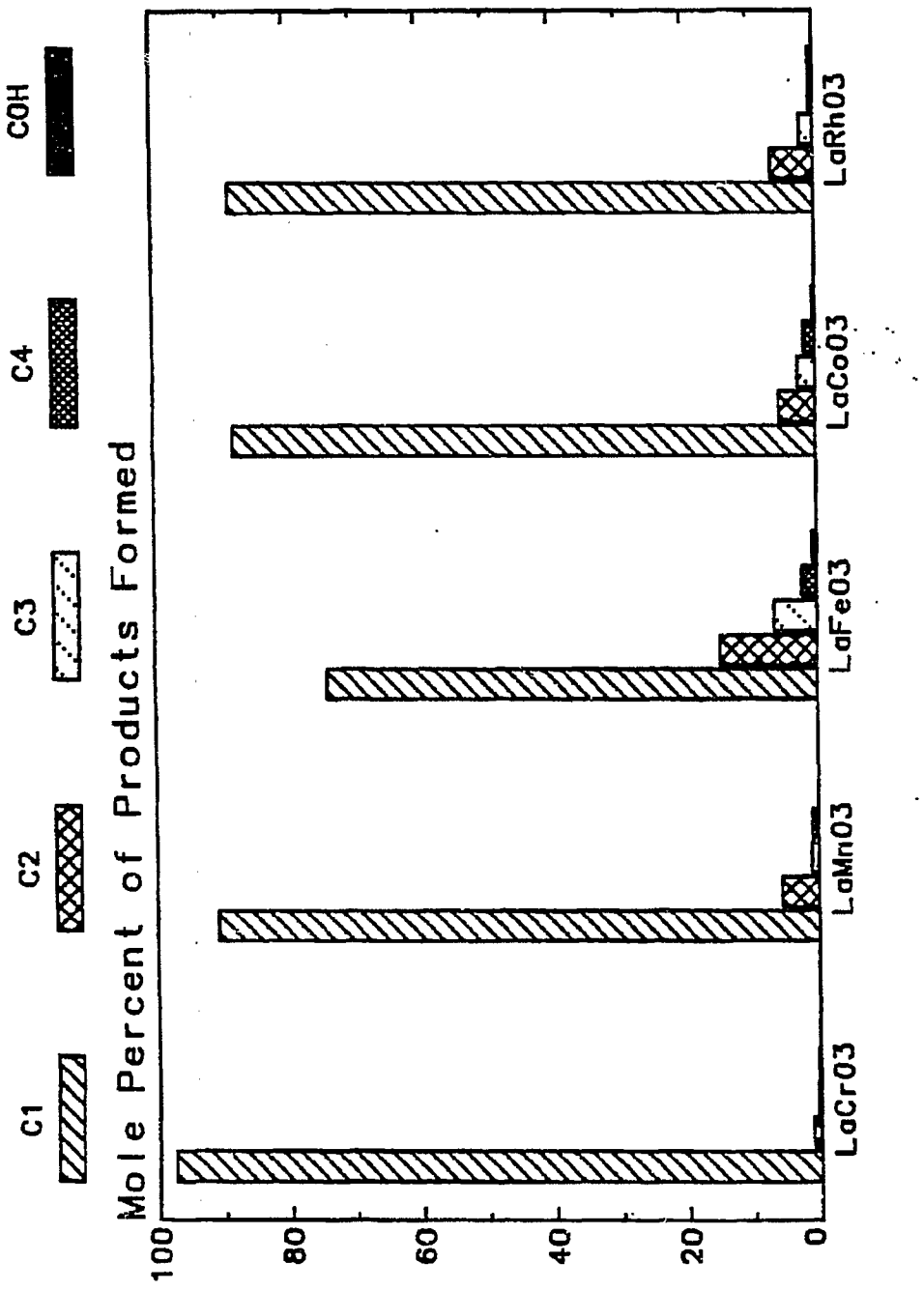

Figure 5.2: Product distribution in the CO hydrogenation reaction for the perovskites $LaRhO_3$, $LaMnC_3$, $LaCoO_3$, $LaFeO_3$ and $LaCrO_3$.

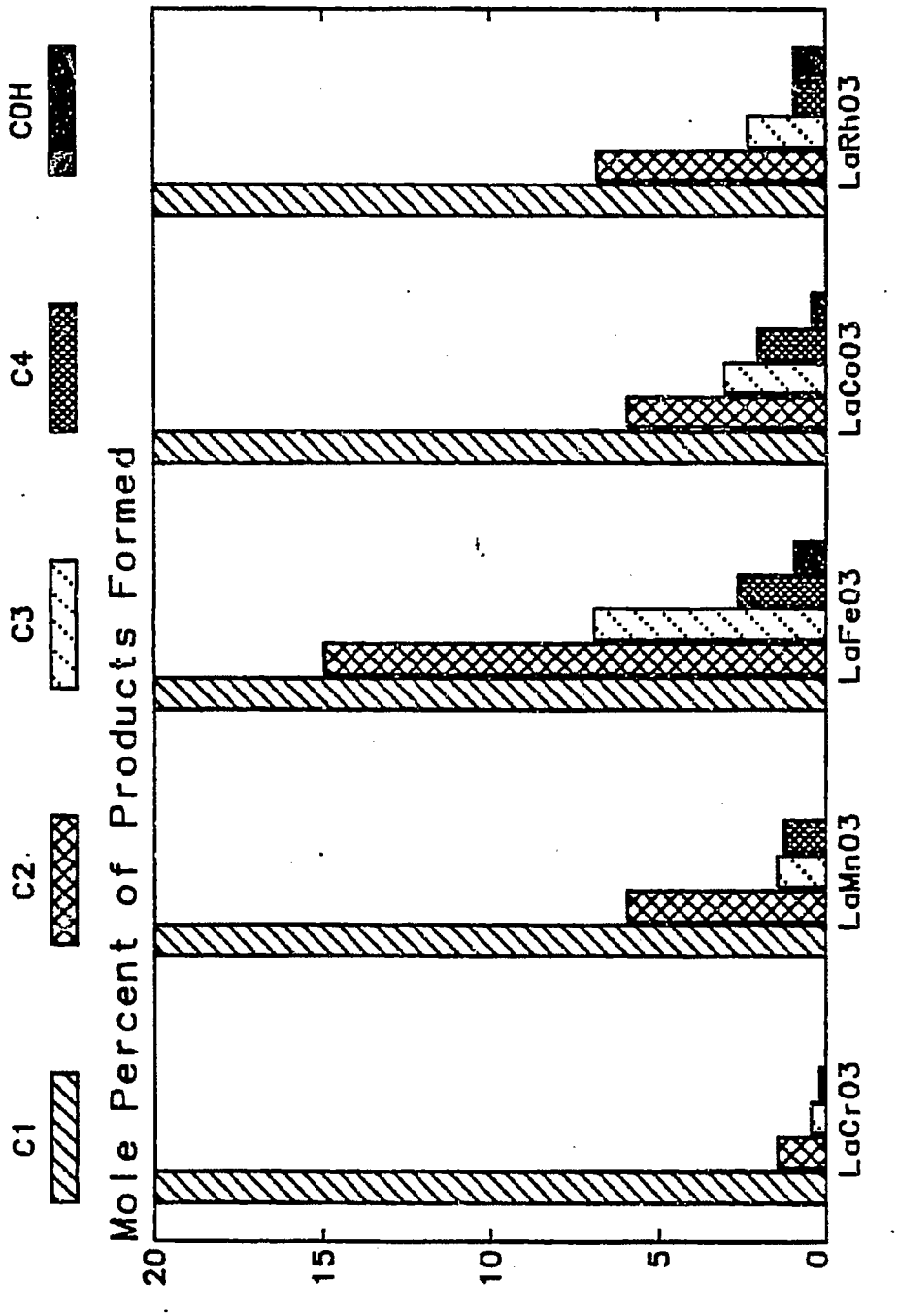

Figure 5.3: Product distribution of C_2, C_3, C_4 and Alcohols in the CO hydrogenation reaction for the perovskite compounds.

Cmpd.	Reaction Product					
	Methane	Ethane	Ethylene	C_3	C_4	COH
$LaCrO_3$	5.8×10^{-4}	5.1×10^{-5}	9.1×10^{-6}	2.2×10^{-5}	1.6×10^{-5}	–
$LaMnO_3$	1.2×10^{-3}	1.3×10^{-4}	1.6×10^{-5}	3.6×10^{-5}	4.6×10^{-5}	–
$LaFeO_3$	6.7×10^{-3}	7.2×10^{-4}	6.4×10^{-4}	9.6×10^{-4}	4.4×10^{-4}	$4.\times10^{-5}$
$LaCoO_3$	9.5×10^{-2}	4.7×10^{-3}	3.2×10^{-3}	1.5×10^{-3}	3.8×10^{-3}	$1.\times10^{-4}$
$LaRhO_3$	6.9×10^{-2}	5.3×10^{-3}	3.0×10^{-3}	3.9×10^{-3}	1.6×10^{-3}	$2.\times10^{-4}$

Table 5.1: Rate of hydrocarbon formation (molecules/site-sec) on perovskite compounds at 250°C, 20 atm.

surface sites were quickly blocked by dissociated CO and hydrocarbons, and that the reaction probably proceeded on the metal and not on a carbon overlayer.

5.2.3 XPS Results

XPS studies were done to probe the oxidation state of the perovskite surface before and after reactions, to determine the catalytically active species. Table 5.2 summarizes the 3d peak positions before and after reactions. In all four samples studied ($LaCrO_3$, $LaFeO_3$, $LaCoO_3$ and $LaRhO_3$), the metal was initially in a high oxidation state (+3) and during the reaction was reduced to the +1 state. This reduction occurred over a period of approximately 15 - 30 minutes after the start of the reaction. None of the samples reduced to the metallic (0) state even after 5 - 6 hours of reaction time. Without the lanthanum oxide matrix, the metals reduce to the metallic state. The perovskite lattice stabilized a slightly oxidized metal. No change in peak position was detected for lanthanum. Figure 5.4 shows a typical full scan obtained for a sample before and after reaction. Studies on other perovskite compounds ($LaMnO_3$, $BaTiO_3$, $LaCoO_3$, $SrTiO_3$, $La_{1-x}Sr_xCoO_3$) report that the

Compound	Binding Energy (eV)	
	Before Reaction	After Reaction
$LaCrO_3$	576.5	575.0
$LaFeO_3$	709.5	707.0
$LaCoO_3$	779.5	778.8
$LaRhO_3$	309.5	307.8

Table 5.2: XPS binding shifts for the perovskite compounds before and after reactions.

B metal can be reduced only at temperatures over 400°C and that this metallic species was slightly active in hydrocarbon hydrogenation and oxidation reactions [14,15,16,17].

5.2.4 $LaRhO_3$

The product accumulation curve (Figure 5.5) shows methane as the major product. Figure 5.6 shows an expansion of the longer (> C_1) hydrocarbon product accumulation curve. Ethylene, C_3 and C_4 show a steady state rate for over 6 hours of reaction time whereas the rate of ethane formation and that of the alcohols decreases after 4 - 5 hours. Interestingly, ethanol formation is initially negligible, but after 2 hours the rate increases and is only slightly less than that of ethylene. Ethanol is detected approximately the same time as the rate of ethane formation decreases and also after 6 - 7 hours when the ethane production starts to level off so does the ethanol production. Ethane may possibly oxidize to form ethanol. For all the hydrocarbons, the reaction rate was positive order in CO and negative order in hydrogen.

Oxidation of the catalyst sample (1 atm, 500°C) increased ethanol formation,

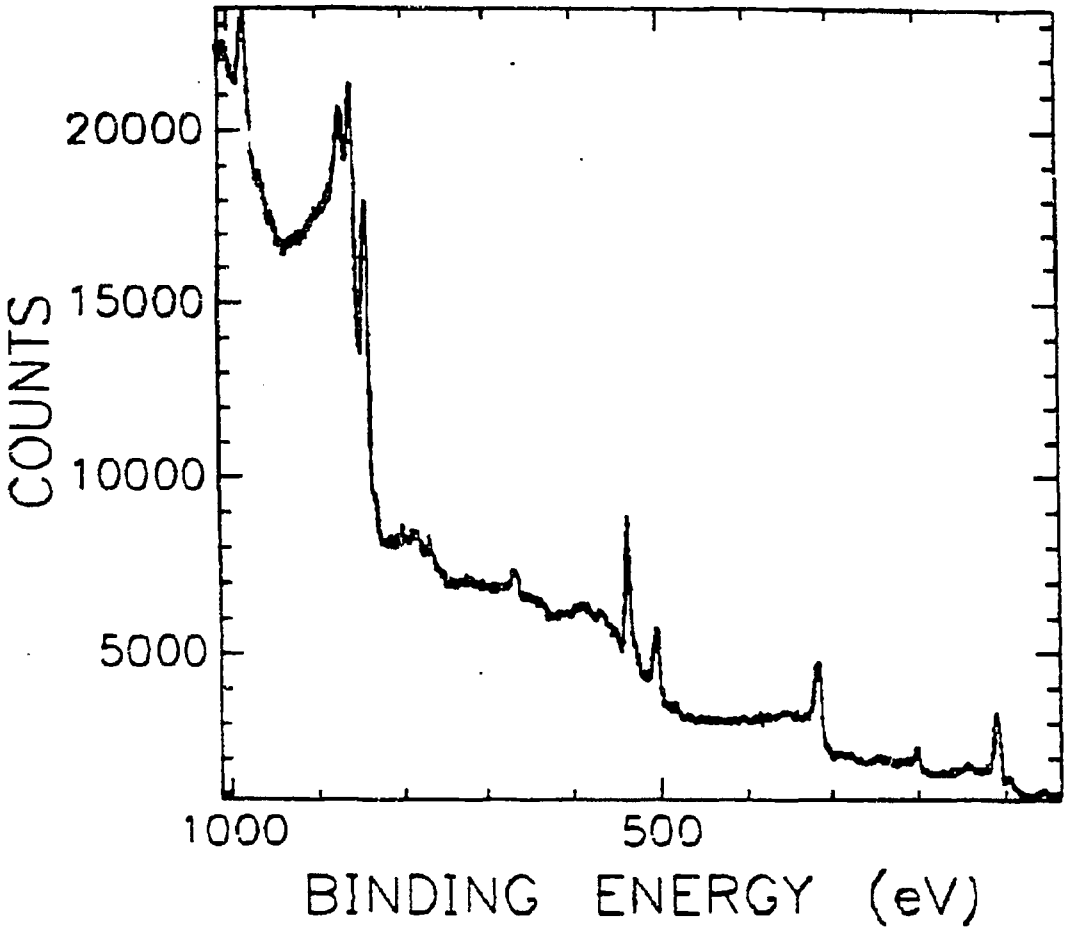

Figure 5.4: A full scan XPS spectra for $LaRhO_3$, after a reaction.

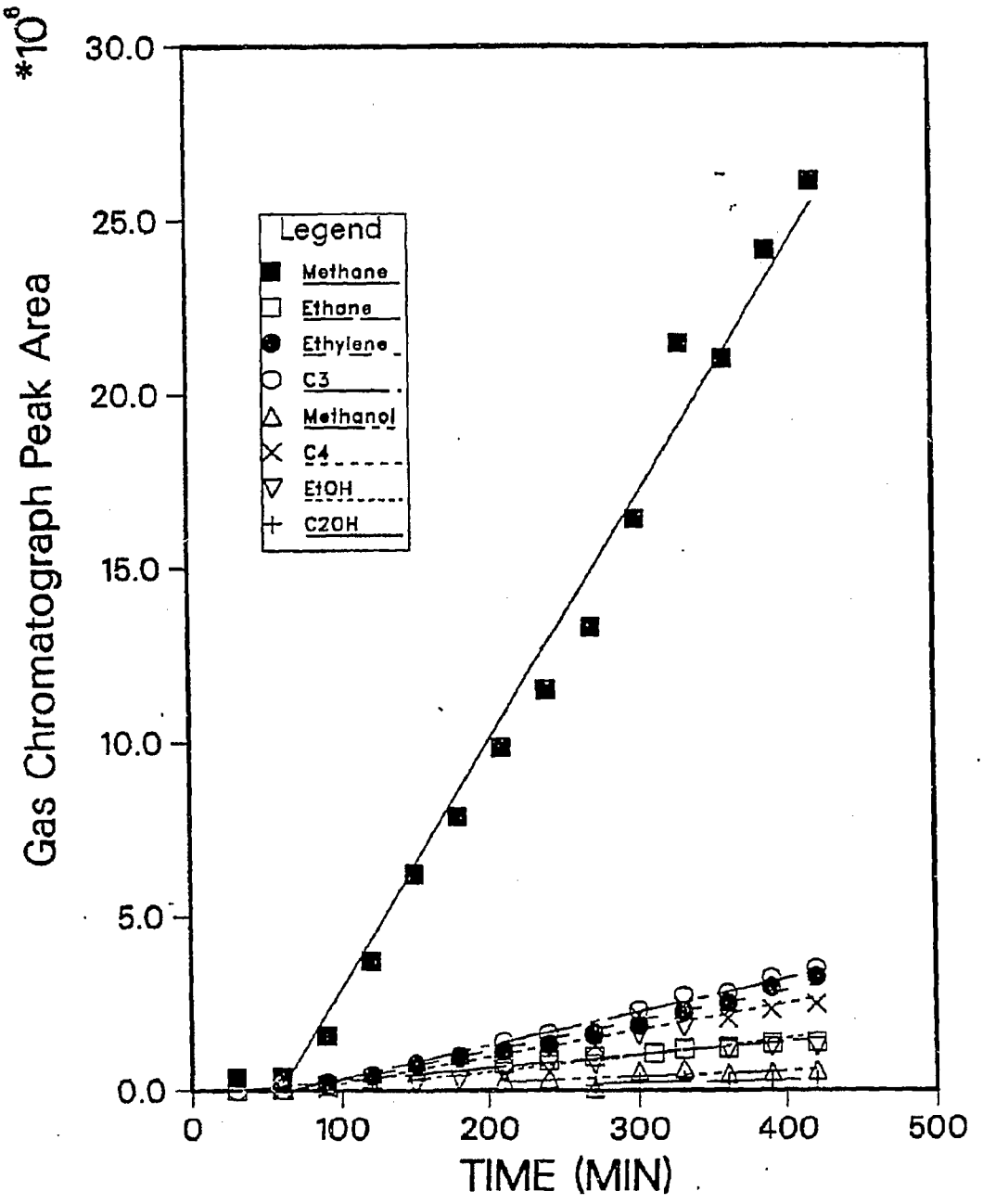

Figure 5.5: Product accumulation curve for $LaRhO_3$, with methane as the major product. Most products are produced for over 5 hours of reaction time.

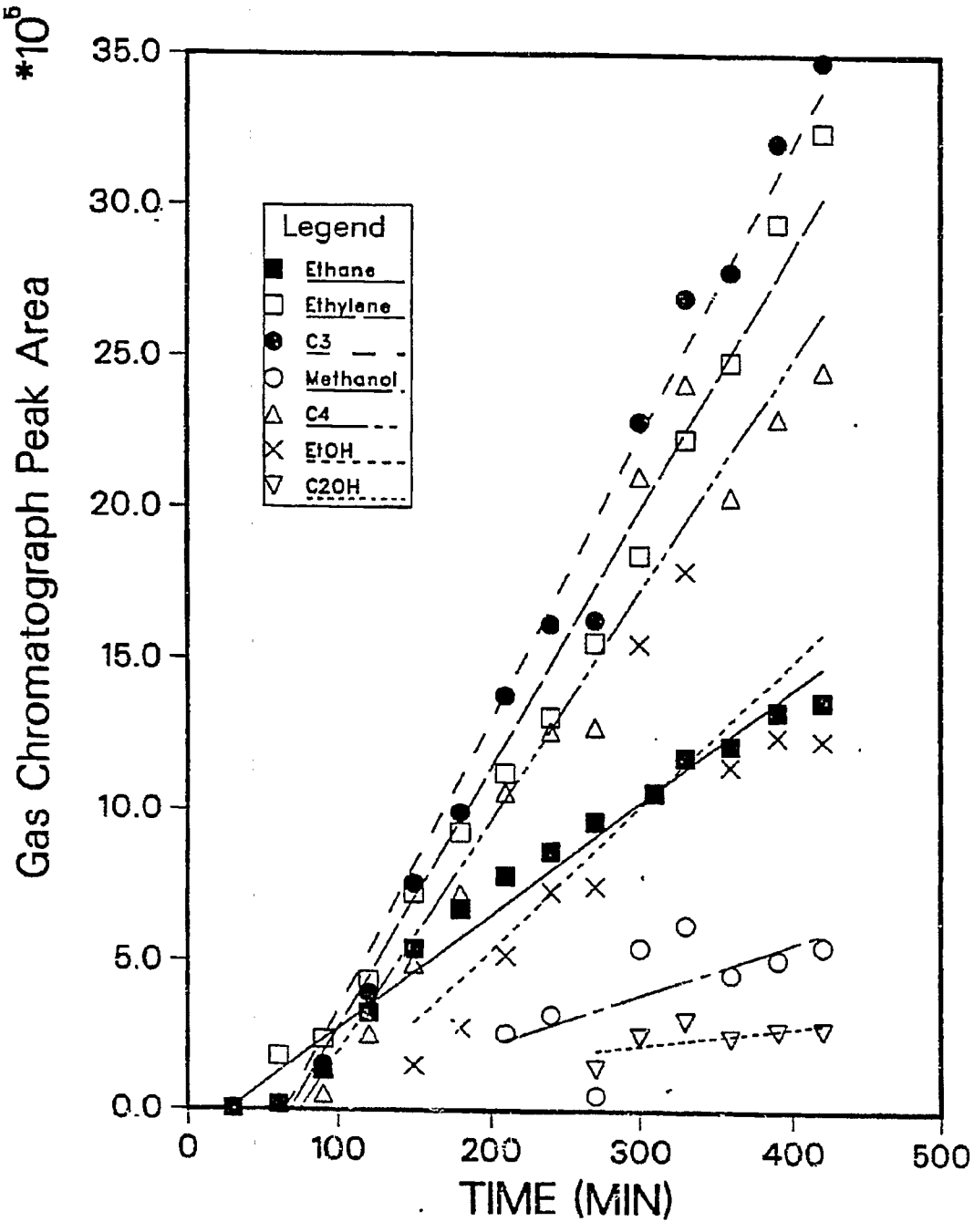

Figure 5.6: Expansion of the product accumulation curve for the longer hydrocarbons (> C_1) over $LaRhO_3$.

suppressed methanol formation, and lowered methane formation by $\sim$ 20% (Figure 5.7). The effect of preoxidation on the other hydrocarbons was minimal.

Studies on the catalytic activity of lanthanum rhodate yielded results quite different than previously reported by Watson *et al.* [12]. They reported an 80 wt% yield of oxygenated products for the CO hydrogenation reaction at temperatures in the range of 225-375°C at 6 atm. In this study we find only a 5 - 9 wt% yield of oxygenates for a similar temperature range and only slightly higher pressures (20 atm). In both their study and ours, the rate of methane and methanol formation vary independently of the formation rate of the other products. This implies that the formation of methanol and methane are occuring by different mechanisms.

XPS characterization of $LaRhO_3$ showed that the initially oxidized (+3) rhodium surface reduced to a +1 state during the reaction (Figure 5.8). Being bonded in the lanthanum oxide matrix kept the rhodium from being completely reduced. After a reaction, cleaning by Ar^+ sputtering and by UHV oxidation (5×10^{-6} torr O_2, 400°C) the rhodium did not become completely oxidized. Only a 1 atm treatment with oxygen accomplished this oxidation.

From these results and other studies on rhodium, it can be concluded that methane forms on metallic or only slightly oxidized ($0 \rightarrow +1$) rhodium with a different mechanism than the other hydrocarbons. Ethanol forms on a more oxidized ($+1 \rightarrow +3$) surface, which the perovskite structure can stabilize under reaction conditions. Other than stabilizing oxidized rhodium, the role of the lanthanum is not well understood. It may also provide mixed interfacial binding sites for hydrocarbon formation, similar to the role of oxide overlayers on palladium (see Chapt. 3).

An important result of this work is that the perovskite compounds exhibit varying catalytic behavior which is critically dependent on the preparation method. We may have produced a different surface composition than Watson *et al.* by

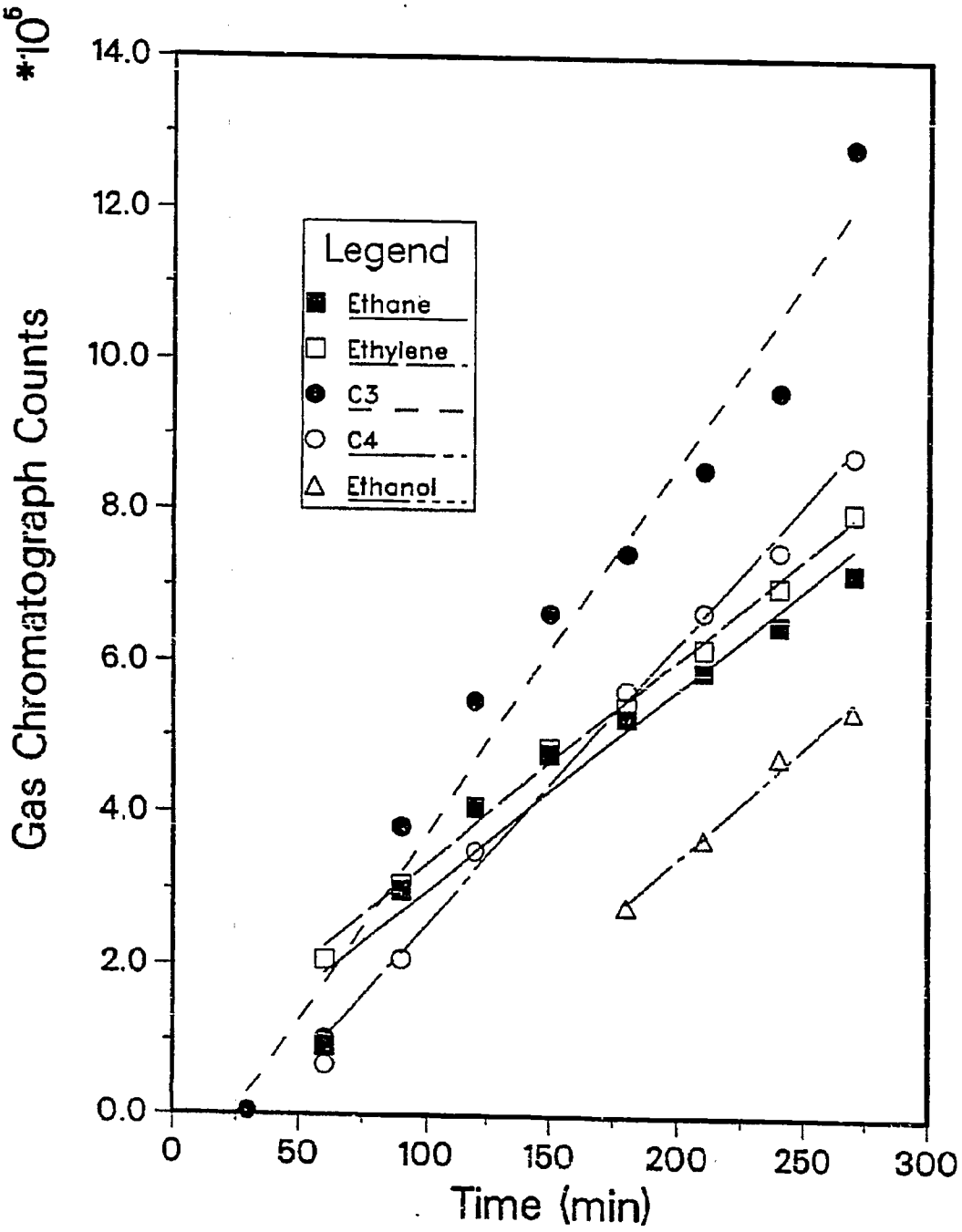

Figure 5.7: Product accumulation curve over $LaRhO_3$ after high pressure oxidation.

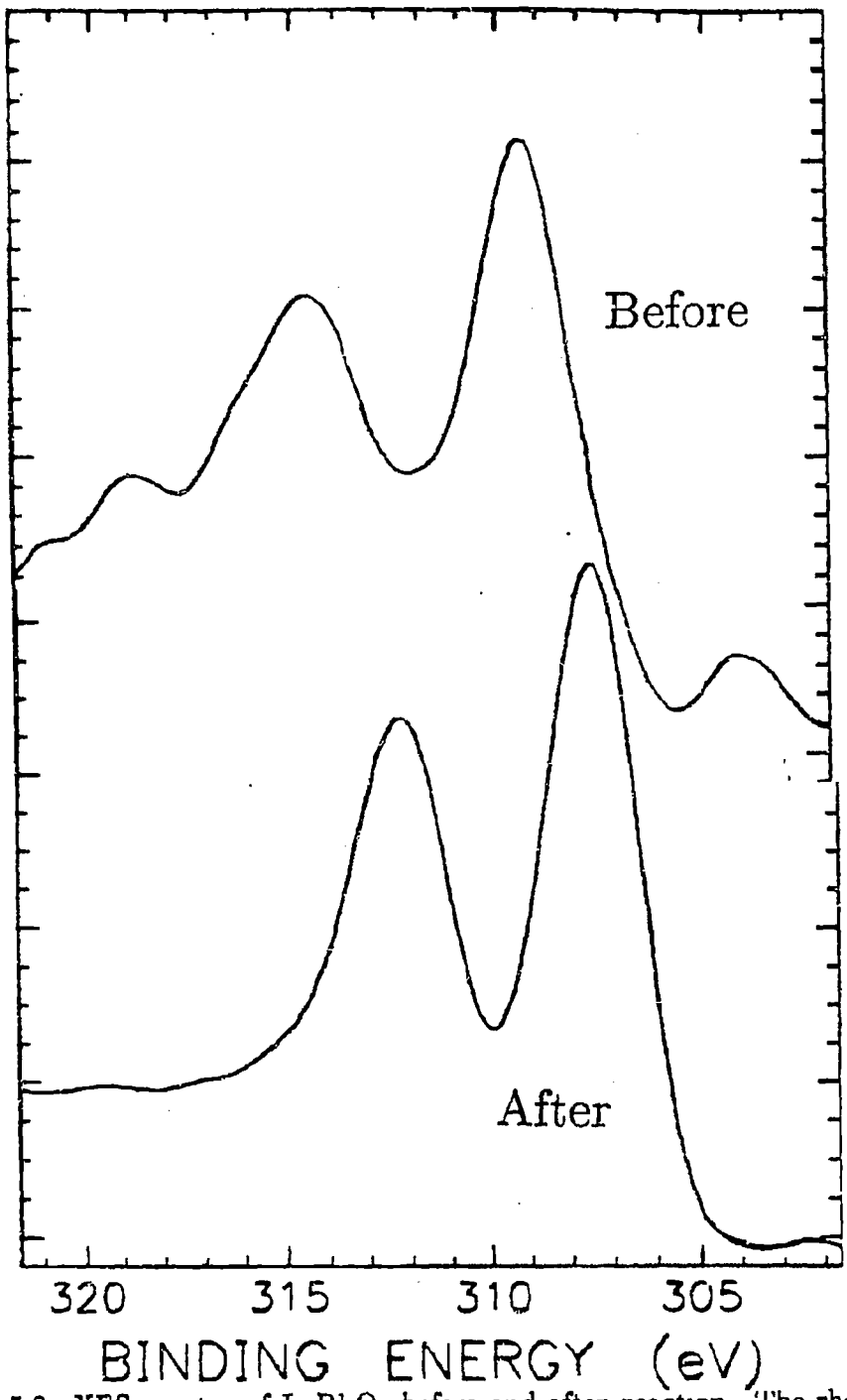

Figure 5.8: XPS spectra of $LaRhO_3$ before and after reaction. The rhodium is reduced from the +3 state but not completely to the metallic state.

pressing our sample into the gold mesh at high pressures rather than drying a wet slurry onto gold foil. The preparation method affects the surface stoichiometry and structure and thereby changes the catalytic behavior. The major difficulty in studying these perovskite compounds is the inhomogeneity of the surface and the difficulty in reproducibly forming a sample with the same surface composition. This was shown by the scatter in the initial rate studies. The ease of preparation and the large number of metals which can be incorporated into the perovskite lattice make this area of solid state chemistry and catalysis and important field for developing tailored stable catalysts.

5.3 Conclusions

The following points summarize the results obtained in this survey of the catalytic activity of perovskite compounds ($LaMO_3$).

- Catalytic activity increases from left to right in the periodic table (Cr > Mn > Fe > Co ~ Rh).
- The major product is methane for all samples.
- $LaFeO_3$ had a higher percentage of longer hydrocarbons in the product distribution.
- All the perovskite compounds reduced to the +1 state during the reaction.

For the $LaRhO_3$ samples studied:

- Alcohol formation does not need Rh^{+3} since catalytic activity remained constant for over 3 hours, even though XPS showed that the metal had been reduced to Rh^{+1}.
- Reoxidation of the sample (1 atm O_2, 450°C) increased the rate of ethanol formation and suppressed methanol formation.

References

[1] R. J. H. Voorhoeve. *Advanced Materials in Catalysis.* Academic Press, New York, 1977.

[2] M. Crespin and W. K. Hall. *J. Catalysis* **69** (1981) 359.

[3] R. J. H. Voorhoeve, D. W. Johnson, J. P. Remeika, and P. K. Gallagher. *Science* **195:4281** (1977) 827.

[4] A. Lauder (E. I. DuPont). *U. S. Patent* **3897367** (1975) .

[5] M. Ichikawa. *Bull. Chem. Soc. Chem. Commun.* (1978) 566.

[6] M. Ichikawa. *J. Catalysis* **56** (1979) 127.

[7] P. C. Ellgen, W. J. Bartley, M. M. Bhasin, and T. P. Wilson. *Advan. Chem. Ser.* **178** (1979) 147.

[8] F. Wunder, H. J. Arpe, E. I. Leupold, and H. J. Schmidt. *U.S. Patent* **4224236** (Hoescht AC) .

[9] M. A. Vannice. *J. Catalysis* **37** (1975) 449.

[10] D. G. Castner, R. L. Blackadar, and G. A. Somorjai. *J. Catalysis* **66** (1980) 257.

[11] P. R. Watson and G. A. Somorjai. *J. Catalysis* **74** (1982) 282.

[12] P. R. Watson and G. A. Somorjai. *J. Catalysis* **72** (1981) 347.

[13] B. Bent. PhD thesis, U. C. Berkeley, Berkeley, CA., 1986.

[14] J. O. Petunchi, M. A. Ulla, J. A. Maracos, and E. A. Lombardo. *J. Catalysis* **70** (1981) 356.

[15] J. L. G. Fierro, J. M. D. Tascon, and L. Gonzalaz Tejuca. *J. Catalysis* **89** (1984) 209.

[16] T. Nakamura, M. Misono, and Y. Yoneda. *J. Catalysis* **83** (1983) 151.

[17] E. Lombardo, K. Tanaka, and I. Toyoshima. *J. Catalysis* **80** (1983) 340.

Chapter 6

CONCLUSIONS AND FUTURE DIRECTIONS

This thesis research has studied the role of surface additives on the catalytic activity and chemisorption properties of palladium single crystals and foils. In particular, the effect of sodium, potassium, silicon, phosphorus, sulfur and chlorine on the bonding of carbon monoxide and hydrogen and on the cyclotrimerization of acetylene on the (111), (100) and (110) faces of palladium was studied in addition to the role of TiO_2 and SiO_2 overlayers deposited on palladium foils in the CO hydrogenation reaction.

The surface characterization and catalytic reactions were performed in a combined ultra-high vacuum/ high pressure chamber equipped with the standard surface analytical techniques. This chamber also included a new high pressure isolation cell mounted inside the chamber capable of attaining pressures of 1800 psi.

On palladium, only in the presence of oxide overlayers (TiO_x, SiO_x) are methane or methanol formed from CO and H_2. The maximum rate of methane formation is attained on a palladium foil where 30% of the surface is covered with titania. Methanol formation can be achieved only if the TiO_x/Pd surface is pretreated in 50 psi of oxygen at 550°C prior to the reaction. Carbon monoxide TPD showed a new high temperature shoulder on the 200°C CO/Pd desorption peak on the TiO_x/Pd

surface which is not present on clean Pd. Pretreating the TiO_x/Pd surface in oxygen led to an additional high temperature (425°C) binding site. The titania overlayers stabilized the palladium oxide relative to the clean and silica covered surfaces in the presence of hydrogen. The TPD and XPS results and the reaction rate studies suggest that methane forms on a stable mixed TiO_x/Pd site whereas methanol, which is produced only during the first few minutes of the reaction, forms on an unstable heavily oxidized TiO_x/Pd surface. Subsequent work should be geared towards fully probing the active site and mechanism for methanol synthesis. From the results of this research it can be seen that an oxidized palladium ion is necessary for methanol formation and possibly the presence of lanthanum oxide or other oxide will stabilize this form of palladium.

The additives (Na, K, Si, P, S, & Cl) affect the bonding of CO and hydrogen and the cyclotrimerization of acetylene to benzene by both structural and electronic interactions. The structural interaction is seen by the structure sensitive bonding of CO on additive doped surfaces. Two examples are: (1) increasing K coverage on Pd(111) increases the CO desorption temperature whereas on the Pd(110) surface the desorption maximum shifts to lower temperature, (2) the differences in CO bonding on phosphorus covered Pd(111) (new peaks) and Pd(100) (slight shift in CO desorption maximum). Surface reconstruction, changes in palladium ensemble size and site blocking are some of the structural changes induced by the additives. The electronic interaction involves the donation or withdrawal of electron density based on the electronegativites of the additives relative to palladium. In general, the electron donating additives increase the desorption temperature of CO and increase the rate of acetylene cyclotrimerization and the electron withdrawing additives decrease the desorption temperature of CO and decrease the rate of benzene formation from acetylene. Further information on the role of additives can be obtained by expanding this study to different reactions and probing the

bonding of small molecules using a variety of surface sensitive techniques.

The perovskite compounds ($LaCrO_3$, $LaMnO_3$, $LaFeO_3$, $LaCoO_3$ and $LaRhO_3$) are active catalysts in the CO + H_2 reaction producing methane, C_2, C_3 and alcohols. The catalytic activity increases moving from left to right in the periodic table (Cr>Mn>Fe>Co~Rh) with $LaFe)_3$ producing the largest percentage of larger hydrocarbons ($>C_1$). The primary role of the lanthanum oxide matrix was in stabilizing the metal in a slightly oxidized (+1) state, which is most likely the active site for alcohol synthesis. Subsequent research in this field should study the effect of catalyst preparation on the surface composition, structure and catalytic activity.

In order to fully characterize and understand any surface chemical phenomena, a wide variety of analytical techniques must be employed. No single technique will answer the myriad of questions but a combination of numerous techniques may well accomplish this goal. The two techniques which would yield the largest amount and least ambiguous information in studying the oxide and additive covered palladium systems and the perovskites are listed below.

Vibrational Spectroscopy EELS or Infra-red Reflection Absorption Spectroscopy (IRRAS) would accurately determine the CO and hydrocarbon bonding configurations in the presence of the adatoms. The development of an in situ high pressure IR cell to monitor the surface species during a reaction would be extremely valuable. This capability would make it easier to determine reaction intermediates and mechanisms without having to infer from UHV measurements.

Scanning Tunneling Microscopy This relatively new technique which can image surfaces on the atomic scale holds great promise in determining the binding sites of adatoms and the growth mechanisms of overlayers. With this information the type and quantity of active catalytic surface sites can

be determined.

Other techniques include Surface Enhanced X-ray Absorption Fine Structure (SEXAFS), Secondary Ion Mass Spectrometry (SIMS).

The goal in studying surface additives is not just to understand their role in specific catalytic systems, but to establish trends and generalized rules for catalysis. Future work should ultimately enhance the predictive power of surface science and catalysis and move the field from an art to a science.

Appendix A

HIGH PRESSURE CELL

This appendix has some pictures and a blueprint of the new high pressure isolation cell developed for studying catalytic reactions.

Figure A.1 Top view of the disassembled components of the high pressure isolation cell. Counterclockwise - 10 inch bottom flange with 4 mini-conflat flanges for connections to gases, pumping and water; 3 inch flange for bottom of outer housing; outer-housing; top of housing and connection for bayonet mount; flange for piston; high pressure cell; assorted o-rings and piston seals; piston; washer; mount for cell·onto 10 inch cell; stainless steel bulkhead and sample holder; spring to force piston up.

Figure A.2 Picture of components arranged in order they would be assembled. The piston seal is attached to groove on the piston which is inserted into the bottom of the cell. The spring and washer are inserted around bottom of the piston and above the flange which is bolted to the high pressure cell. The bottom of the piston, which goes through the flange attached to the cell, is bolted to another flange which is bolted to the outer housing (not shown). This unit sits on a small pedestal which is attached to the bottom flange.

Figure A.3 Side view of the high pressure cell. On the cell (l to r) the connections are for differential pumping, cooling jacket water in, cooling jacket

water out to bottom jacket, reactant gas in, reactant gas out, nitrogen line for pressurizing piston, cooling jacket water in from top jacket, cooling jacket water out, differential pumping for volume below piston.

Figure A.4 Top view showing dove-tail grooves for viton o-rings which are the sealing surface for the manipulator against the cell. The differential pumping hole can be seen in the middle groove in the side where the lines are attached to the cell.

Figure A.5 View of the stainless steel bulkhead with thermocouple and electrical feedthroughs welded in. The four teeth of the manipulator are grabbed in the bayonet mount (right) attached to the outer housing.

Figure A.6 View of outer housing and bayonet mount. The housing was machined to minimize mass.

Figure A.7 Close up view of piston assembly used through which the nitrogen pulls down the outer housing sealing the manipulator against the o-rings of the high pressure cell.

Figure A.8 Assembled high pressure cell.

Figure A.9 Assembled high pressure cell.

Figure A.10 Blueprint of the manipulator and high pressure cell.

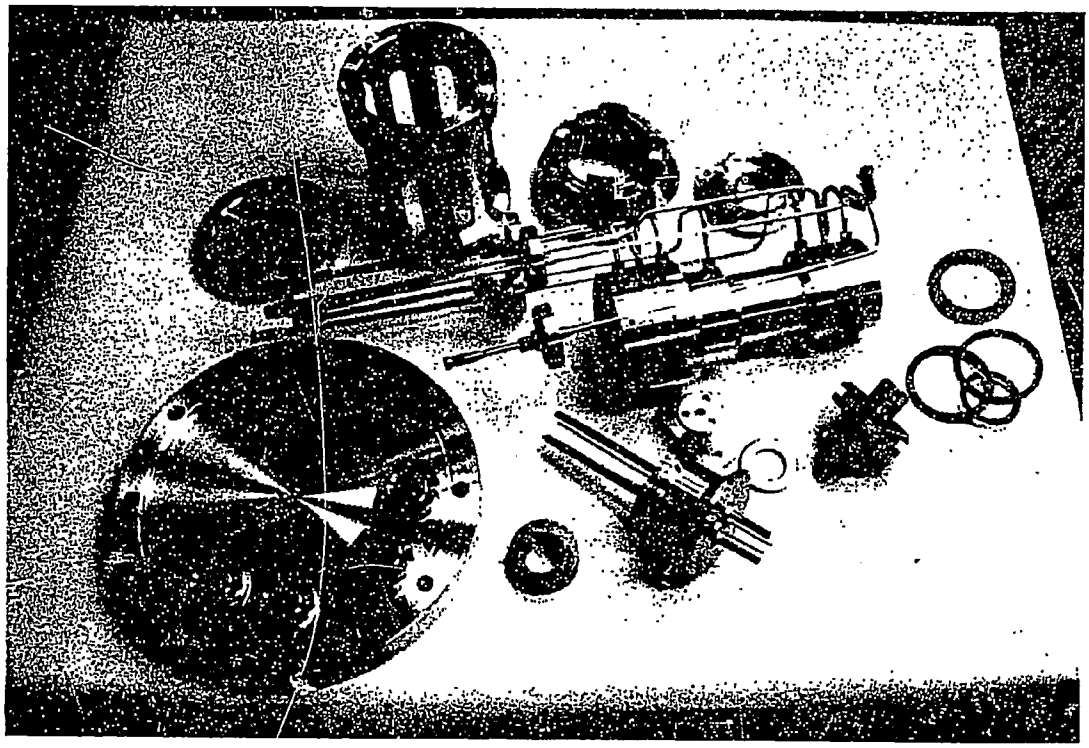

XBB 874-3321

Figure A.1:

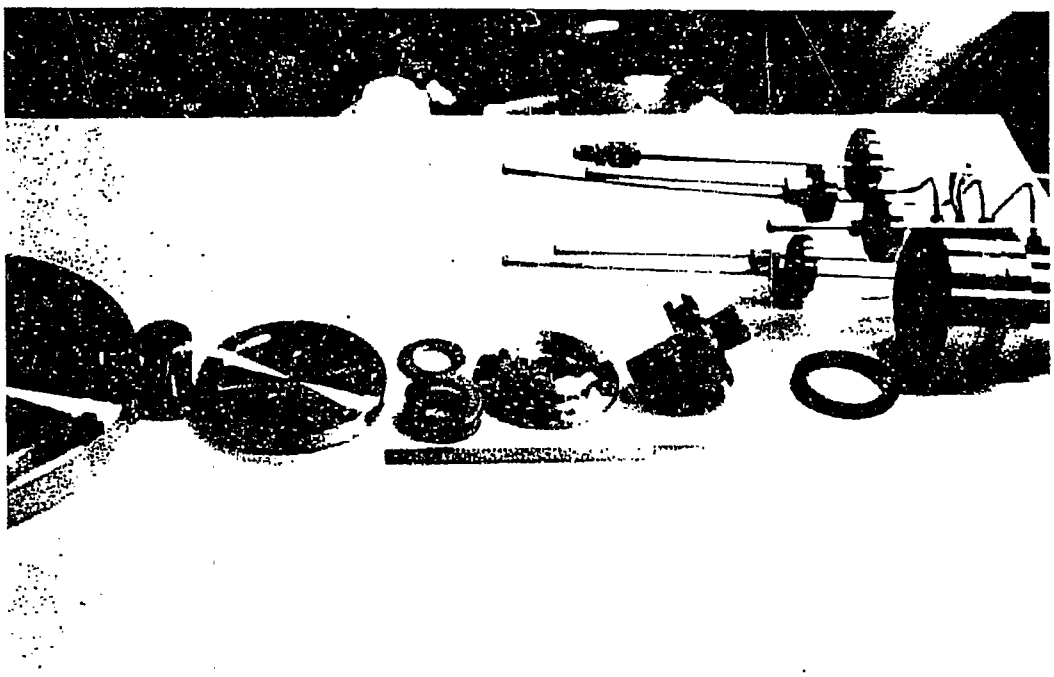

XBB 874-3318

Figure A.2:

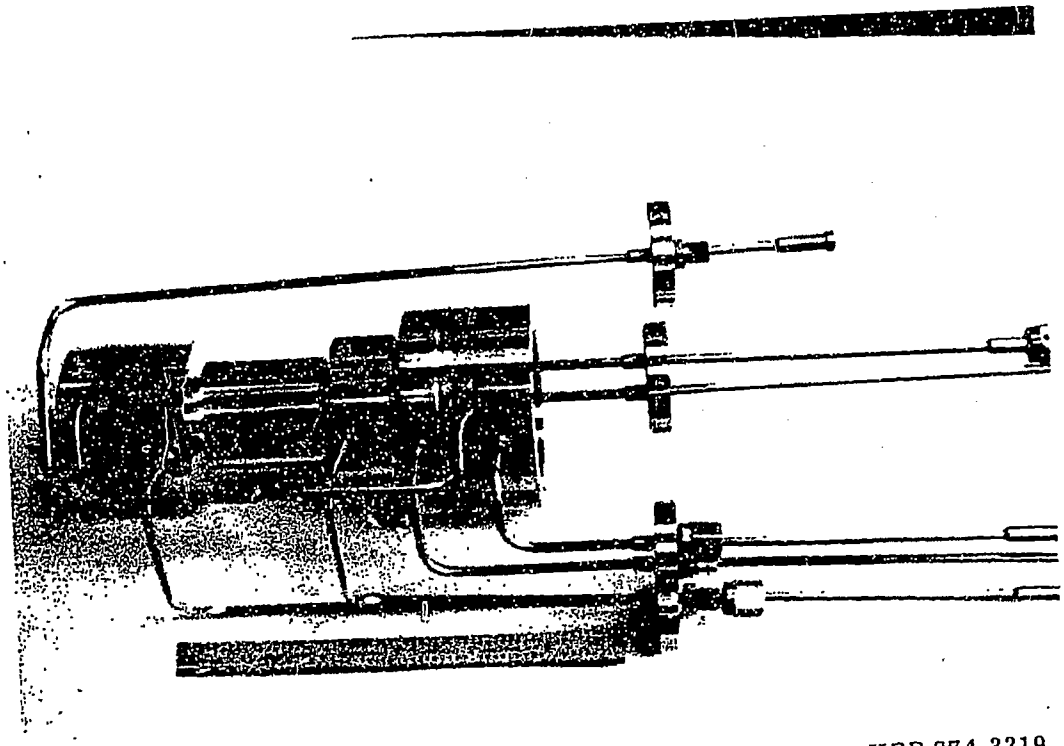

XBB 874-3319

Figure A.3:

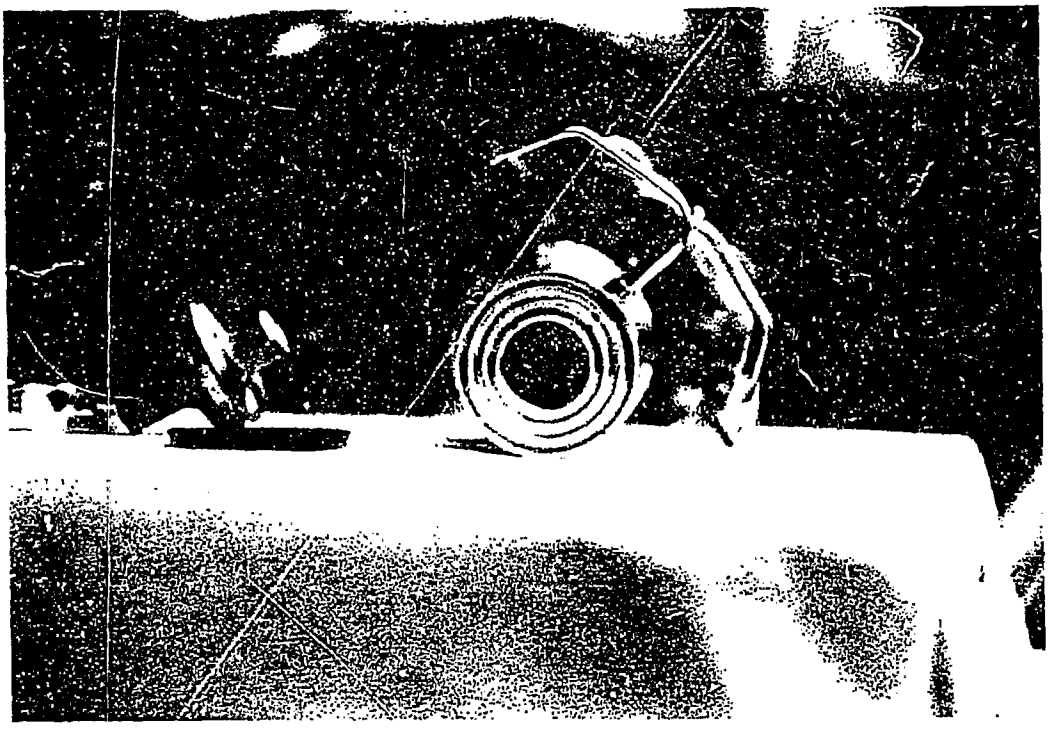

XBB 874-3317

Figure A.4:

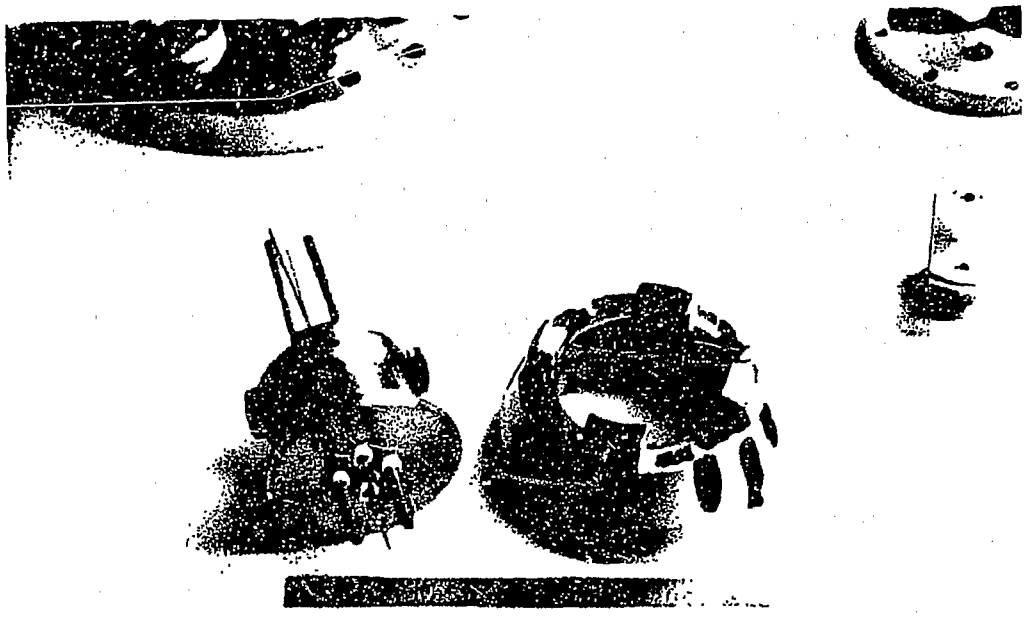

XBB 874-3315

Figure A.5:

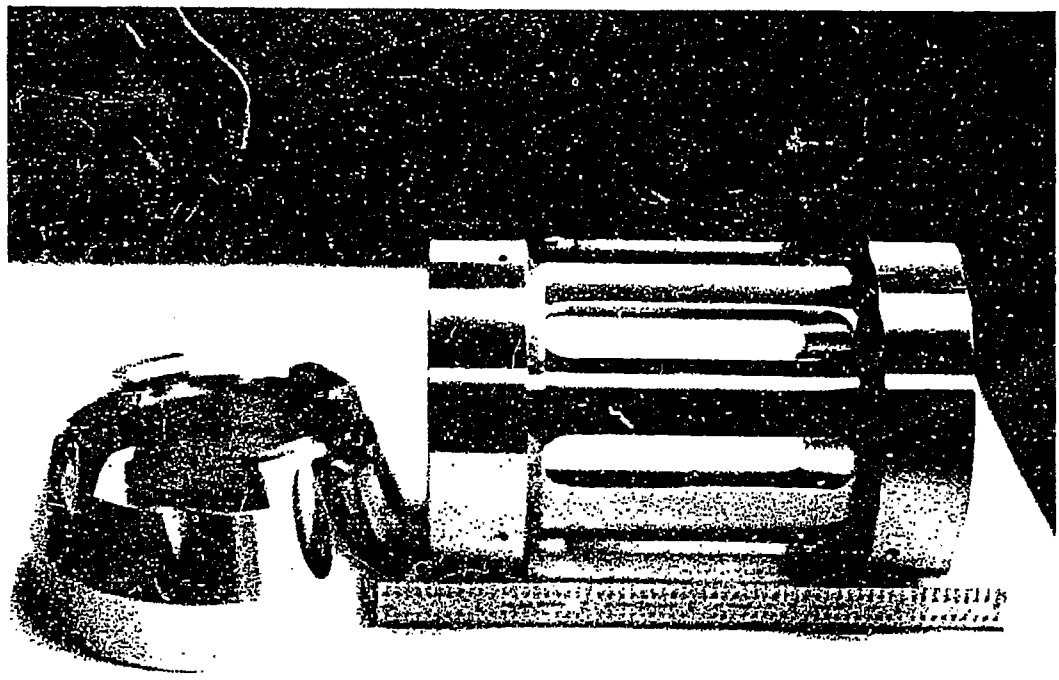

XBB 874-3320

Figure A.6:

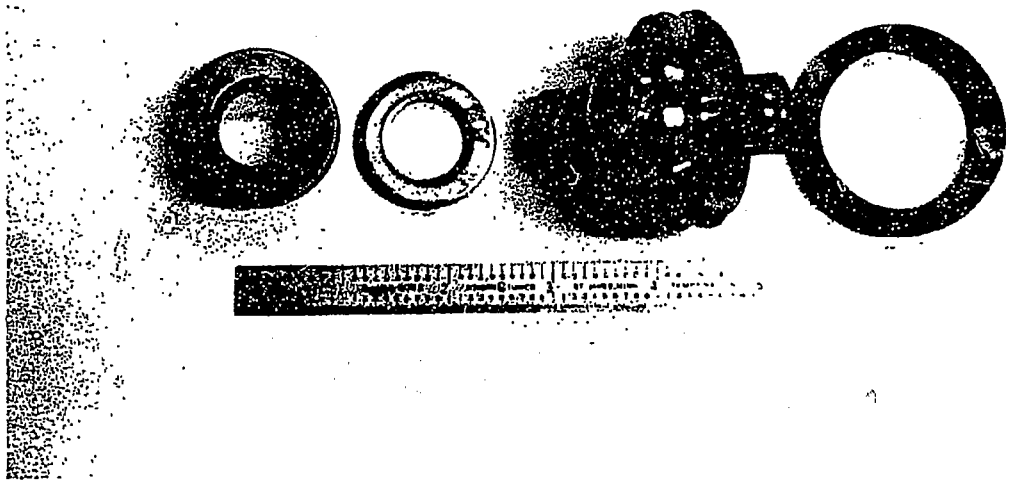

XBB 874-3316

Figure A.7:

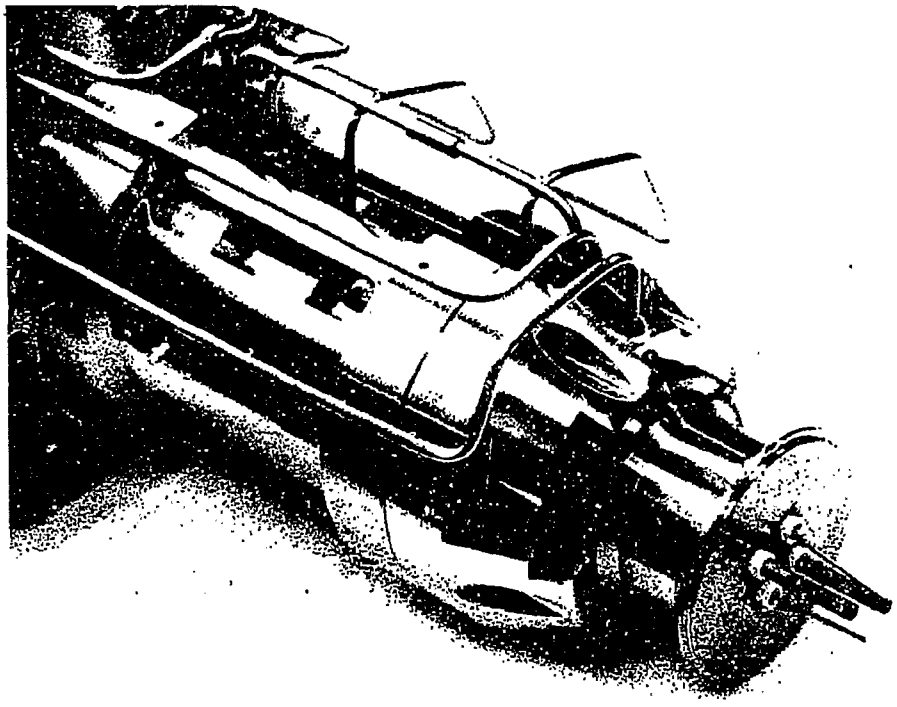

XBB 876-4909

Figure A.8:

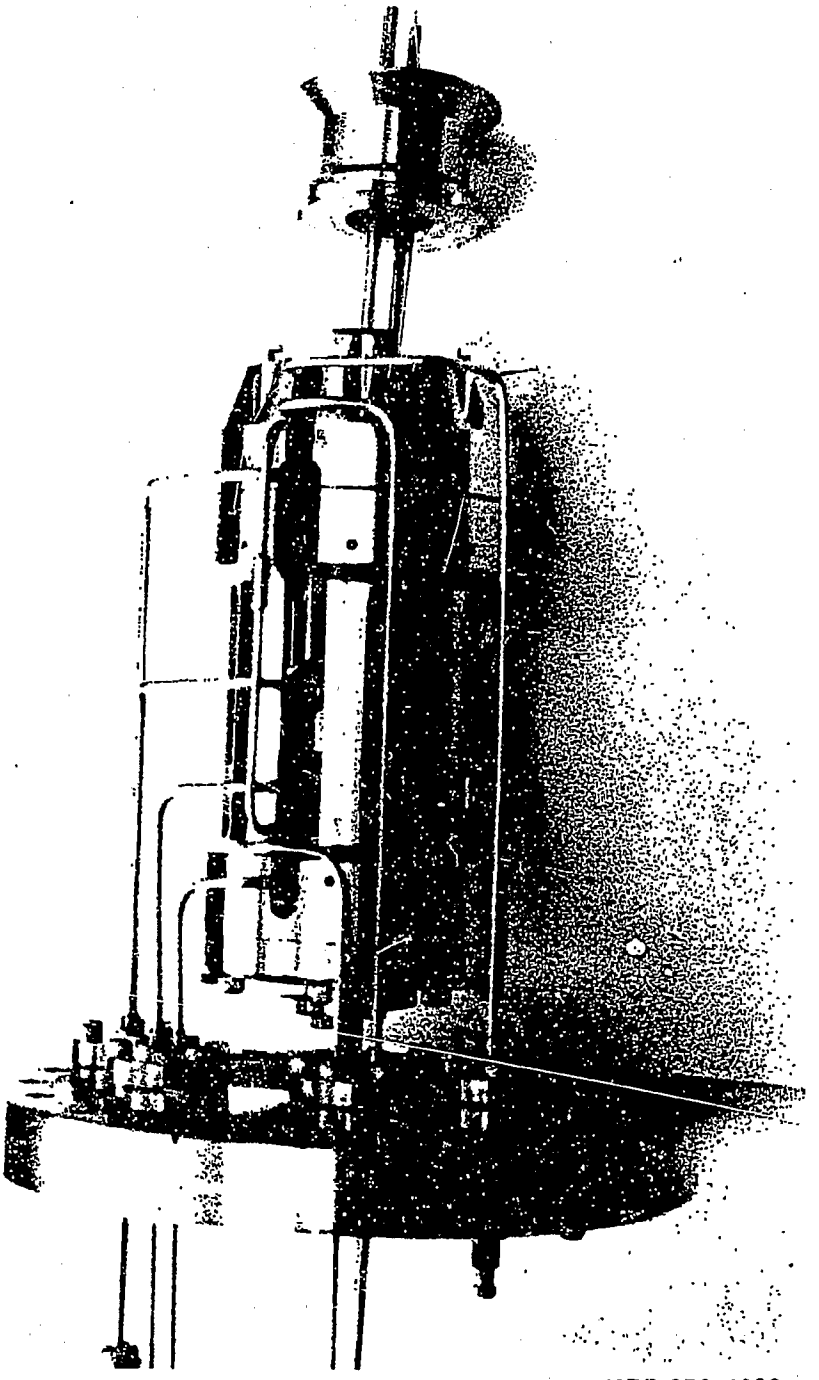

Figure A.9: XBB 876-4908

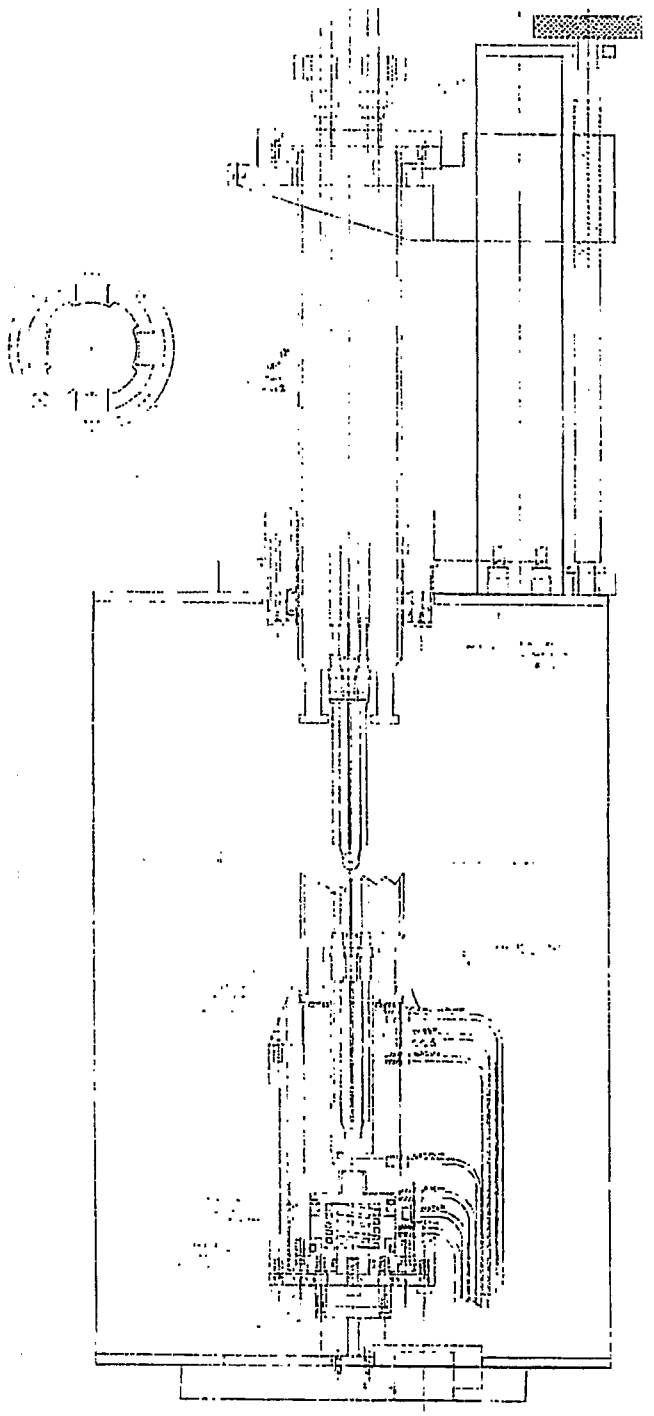

Figure A.10:

Appendix B

CURVE FITTING ALGORITHM

The algorithm and program listing (RPLOT) [1] to fit gaussian peaks for the XPS peaks is presented below.

Known: f_i, g_i, h_i (functions) where i is index to points

Find: a, b, c

So that $e_i \cong af_i + bg_i + ch_i$

where e_i are the experimental data points.

Minimize error: $\xi = \sum_{i=0}^{300} [e_i - (af_i + bg_i + ch_i)]^2 = \sum \varepsilon^2$

with respect to unknowns a, b and c.

Three equations:

$$\frac{\partial \xi}{\partial a} = 2\sum_{i=0}^{300}(e_i + af_i - bg_i - ch_i)(-f_i) = 0$$

$$\frac{\partial \xi}{\partial b} = 2\sum_{i=0}^{300}(e_i + af_i - bg_i - ch_i)(-g_i) = 0$$

[1] Graphics and data manipulation program developed by Craig G. Shaefer, Rowland Institute of Science, Cambridge, MA

$$\frac{\partial \xi}{\partial c} = 2\sum_{i=0}^{300}(e_i + af_i - bg_i - ch_i)(-h_i) = 0$$

Work out three equations:

$$\begin{aligned}
a\sum_{i=0}^{300} f_i^2 + b\sum_{i=0}^{300} g_i f_i + c\sum_{i=0}^{300} h_i f_i &= \sum_{i=0}^{300} e_i f_i \\
a\sum_{i=0}^{300} f_i g_i + c\sum_{i=0}^{300} g_i^2 + c\sum_{i=0}^{300} h_i g_i &= \sum_{i=0}^{300} e_i g_i \\
a\sum_{i=0}^{300} f_i h_i + b\sum_{i=0}^{300} g_i h_i + c\sum_{i=0}^{300} h_i^2 &= \sum_{i=0}^{300} e_i h_i
\end{aligned}$$

In matrix form:

$$\begin{bmatrix} \sum f_i^2 & \sum g_i f_i & \sum h_i f_i \\ \sum f_i g_i & \sum g_i^2 & \sum h_i g_i \\ \sum f_i h_i & \sum g_i h_i & \sum h_i^2 \end{bmatrix} \begin{bmatrix} a \\ b \\ c \end{bmatrix} = \begin{bmatrix} \sum e_i f_i \\ \sum e_i g_i \\ \sum e_i h_i \end{bmatrix}$$

$$\mathrm{M} \quad \mathrm{A} = \mathrm{K}$$

$$\mathrm{A} = \mathrm{M}^{-1} \quad \mathrm{K}$$

Program Listing for RPLOT:

```
MAN CAL "(1/($B1*2.4))*EXP(-1*(X-$X1)**2/(2*($B1**2)))" TO W
MAN COP W V
MAN POW W 2.
MAN INT W TO U
SET VAR "$" R 1 U111

MAN CAL "(1/($B2*2.4))*EXP(-1*(X-$X2)**2/(2*($B2**2)))" TO Z
MAN COP Z U
MAN POW Z 2.
MAN INT Z TO W
SET VAR "$" R 2 W111
```

```
MAN CAL "(1/($B1*2.4))*EXP(-1*(X-$X1)**2/(2*($B1**2)))" TO W
MAN CAL "(1/($B2*2.4))*EXP(-1*(X-$X2)**2/(2*($B2**2)))" TO Z
MAN MUL W Z TO Z
MAN INT Z TO W
SET VAR "$" R 3 W111

MAN CAL "(1/($B1*2.4))*EXP(-1*(X-$X1)**2/(2*($B1**2)))" TO W
MAN MUL W Y TO W
MAN INT W TO V
SET VAR "$" R 4 V111

MAN CAL "(1/($B2*2.4))*EXP(-1*(X-$X2)**2/(2*($B2**2)))" TO Z
MAN MUL Z Y TO Z
MAN INT Z TO V
SET VAR "$" R 5 V111

CAL
$S1=$R1
$S2=$R2
$S3=$R3
$S4=$R4
$S5=$R5

$T1=-1*($R4 * $R2 - $R5 * $R3)/($R3**2 - $R1 * $R2)
$T2= ($R4 * $R3 - $R5 * $R1)/($R3**2 - $R1 * $R2)
E
```

```
MAN CAL "(1/($B1*2.4))*EXP(-1*(X-$X1)**2/(2*($B1**2)))" TO W
MAN SCA W $T1 TO W
MAN CAL "(1/($B2*2.4))*EXP(-1*(X-$X2)**2/(2*($B2**2)))" TO Z
MAN SCA Z $T2 TO Z
MAN ADD W Z TO U
SYM +
PLO X W
SYM *
PLO X Z
SYM LIN
PLO X U
SYM DOT
PLO
LOG OFF
```

U.S. DEPARTMENT OF COMMERCE
Technology Administration
National Technical Information Service
Springfield, VA 22161 (703) 605-6000